이학박사 학위논문

Preparation of Well-Defined Nanostructures by Crystallization-Driven Self-Assembly of Simple Conjugated Homopolymers

간단한 혼성화 동종 중합체의 결정화 주도 자기조립을 이용한 잘 정의된 나노구조의 제조

2019 년 2 월

서울대학교 대학원
화학부 유기화학 전공
최 인 호

Preparation of Well-Defined Nanostructures by Crystallization-Driven Self-Assembly of Simple Conjugated Homopolymers

지도교수 최 태 림

이 논문을 이학박사 학위논문으로 제출함

2019 년 2 월

서울대학교 대학원

화학부 유기화학 전공

최 인 호

최인호의 이학박사 학위논문을 인준함

2018 년 12 월

위 원 장 이 동 환 (인)

부위원장 최 태 림 (인)

위 원 손 병 혁 (인)

위 원 김 경 택 (인)

위 원 임 지 우 (인)

Abstract

Preparation of Well-Defined Nanostructures by Crystallization Driven Self-Assembly of Simple Conjugated Homopolymers

Inho Choi
Organic Chemistry in Department of Chemistry
The Graduate School
Seoul National University

Self-assembly of block copolymers in solution was well-known for many decades, and various kinds of nanostructures could be formed by the different combinations of core and corona block with many strategies. However, there were few examples using simple peptide units as a building block for the self-assembled nanostructures. Therefore, the thesis demonstrates the development of effective strategies for the preparation of well-defined nanostructures by simple peptides or peptide substituted block copolymers with controlled size.

Also the thesis demonstrates the nanostructures and chemosensor ability of the water-soluble block copolymers containing poly (naphthylene vinylene) (PNV) core block with some polyethylene glycol (PEG)-attached soluble corona blocks. The block copolymer showed good efficiency of the chemosensor.

Key words: Peptide, Self-Assembly, Water-soluble nanostructure, Chemosensor

Student Number: 2012-20290

Table of Contents

Chapter 1. Introduction

1-1. *In situ* Nanoparticlization

Self-assembly of a block copolymers (BCPs) in a selective solvent for an insoluble core block has been widely investigated for many decades[1-3], and various kinds of self-assembled nanostructures including nanospheres[4], nanovesicles[5], nanofibers[6], nanoribbons[7], nanotubes[8], nanosheets[9], and many other complex nanostructures[10,11] could be generated with variable insoluble core and soluble corona blocks respectively. However, most of the nanostructures made by BCPs necessarily required some post-synthetic processes, such as the introduction of glue molecules[12], aging[13], dialysis[14], change in temperature[15], or re-dissolution in selective solvents[16]. In general, these kinds of tedious post-treatments are unavoidable because of the weak crystallinity of the core blocks in the BCPs. Then, this problem was partially got solved by polymerization-induced self-assembly (PISA) process[17]. However, the nanostructures by PISA process are not thermodynamically stable because the driving force to form the nanostructures was not strong enough (**Figure 1.1**). Furthermore, the morphology of nanostructures was quite limited, such as micelles, vesicles, or cylinders (**Figure 1.2**).

For that reason, changing the core block to more crystalline polythiophene (PT)[10,18], poly(*para*-phenylene vinylene) (PPV)[11] or non-substituted polyacetylene (PA)[19] could induce strong driving force to form the various kinds of self-assembled nanostructures by *in situ* manners. This method is called *in situ* nanoparticlization of conjugated polymers (INCP), and it takes advantage of the strong $\pi-\pi$ interactions with insolubility of the conjugated core as the driving force for the self-assembly (**Figure 1.1**). Such strong interactions highly fixed the shape of the nanostructures during the polymerization, resulting in undulated nanorod (nanocaterpillar)[18,19], nanostar[10], and nanofractals[11]

grown by step-growth attachment of micelle structures (Figure 1.3). However, it was hard to control the size and dimension of these nanostructures during the INCP process because of the fast aggregation of the conjugated blocks.

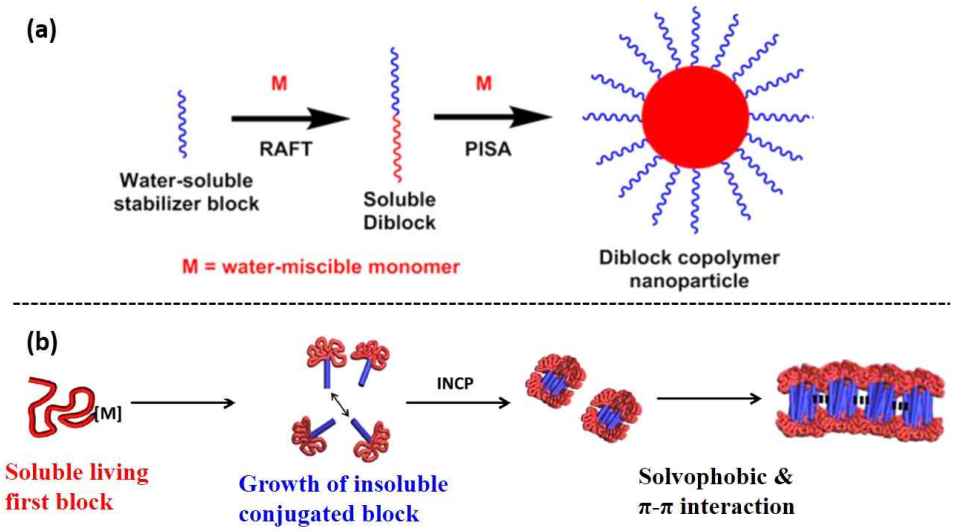

Figure 1.1. Schematic illustration of (a) PISA process[17] and (b) *in situ* nanoparticlization of conjugated polymers process (INCP)[10] to form various nanostructures of the block copolymers in solution.

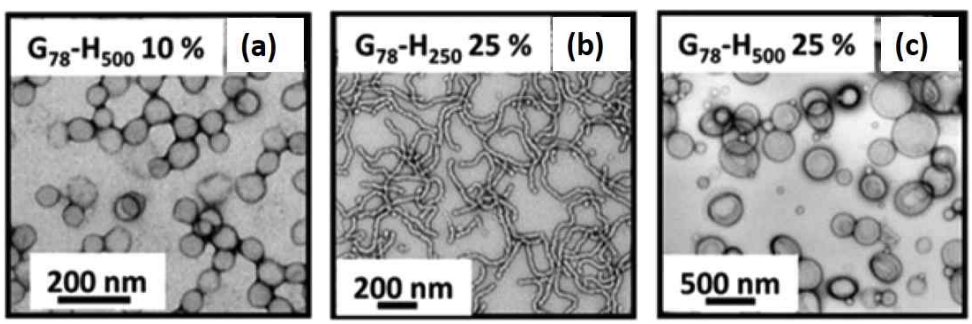

Figure 1.2. (a-c) TEM images of various kinds of nanostructures made by poly(glycerol monomethacrylate-*b*-2-hydroxypropyl methacrylate) with different block ratios in water (weight percent) by PISA[17].

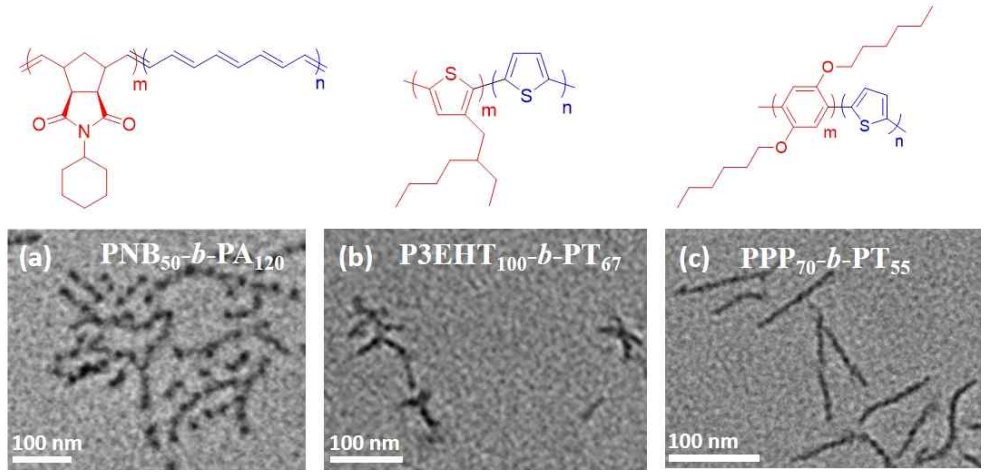

Figure 1.3. (a–c) TEM images of the nanostructures (a) in chloroform (0.05 mg/mL), (b) in toluene (0.05 mg/mL), and (c) in chlorobenzene (0.05 mg/mL) made by INCP[10,18,19].

1-2. Crystallization-Driven Self-Assembly

Most of the nanostructures which were formed by a self-assembly process of BCPs in a selective solvent for the core block usually had a problem of control the dimension of nanostructures with a broad length or area distribution[20]. This is a likely the lack of crystallinity of core-forming block or the irregular and slow rate of the self-nucleation process. However, there were several reports about the elongation of pre-existing small cylindrical micellar fragments called "seeds" which composed of some crystalline poly(ferrocenyl dimethylsilane) (PFDMS)[21], poly(ε -caprolactone) (PCL)[22], polyfluorene[23], poly(L-lactide)[24], and PPV[25] cores occurred in solution upon further epitaxial growth to the exposed crystalline edges at each micelle core with a unimer which was dissolved like a free polymer state at solution. Ultrasonication of polydisperse nanofibers could form the seed micelles that could act as initiators for the further epitaxial bidirectional growth of the micelles with low length dispersities. Under the seeded growth conditions, the increasing the length of nanofibers could be controlled by the ratio between the seeds and the unimers. This process was similar with a living polymerization process, and it could be called "living crystallization-driven self-assembly (CDSA) (**Figure 1.4**)."

The alternative method of living CDSA route to monodisperse nanofibers in solution is *via* "self-seeding" protocol[26]. This process involves the mild water-bath sonication of polydisperse nanofibers to form shorter micelles that are longer than those used for the seeded growth. Thermal annealing of the resulting shorter micelles at a constant temperature (typically between at 30 and 75 ℃ about 30 minutes)[27] then results in dissolution of the seeds to the unimers, as these exhibit a lower T_m near the annealing temperature. Then, the

unimers are crystallized to the surviving seeds which did not dissolved at annealing temperature, and cooling at room temperature produced monodisperse nanofibers. Furthermore, higher annealing temperature could produce more unimers with less amount of seeds, so the length control of nanofibers could be tuned by the annealing temperatures (Figure 1.5).

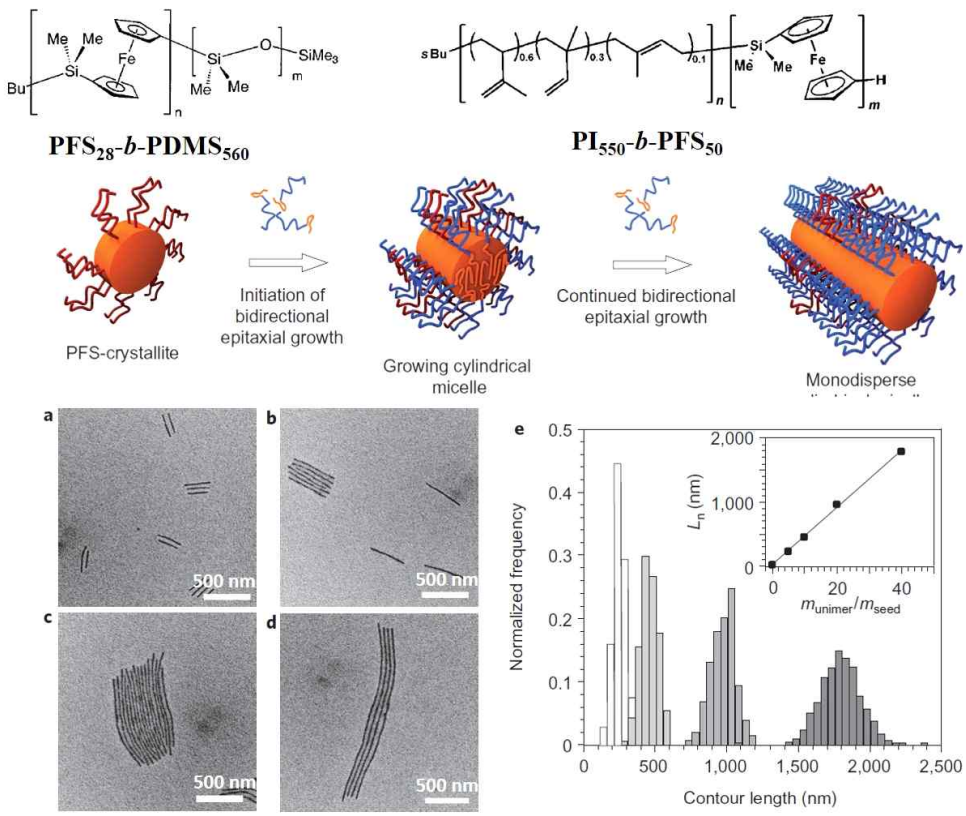

Figure 1.4. Schematic illustration of CDSA *via* seeded growth made by PFS_{28}-*b*-$PDMS_{560}$ seed in *n*-hexane and PI_{550}-*b*-PFS_{50} unimer in THF[21]. (a-d) TEM images of the nanofibers by seeded growth. (a) seed: unimer= 1:5, (b) 1:10, (c) 1:20, and (d) 1:40. (e) The average length distribution of the seeded growth nanofibers by increasing seed and unimer ratio.

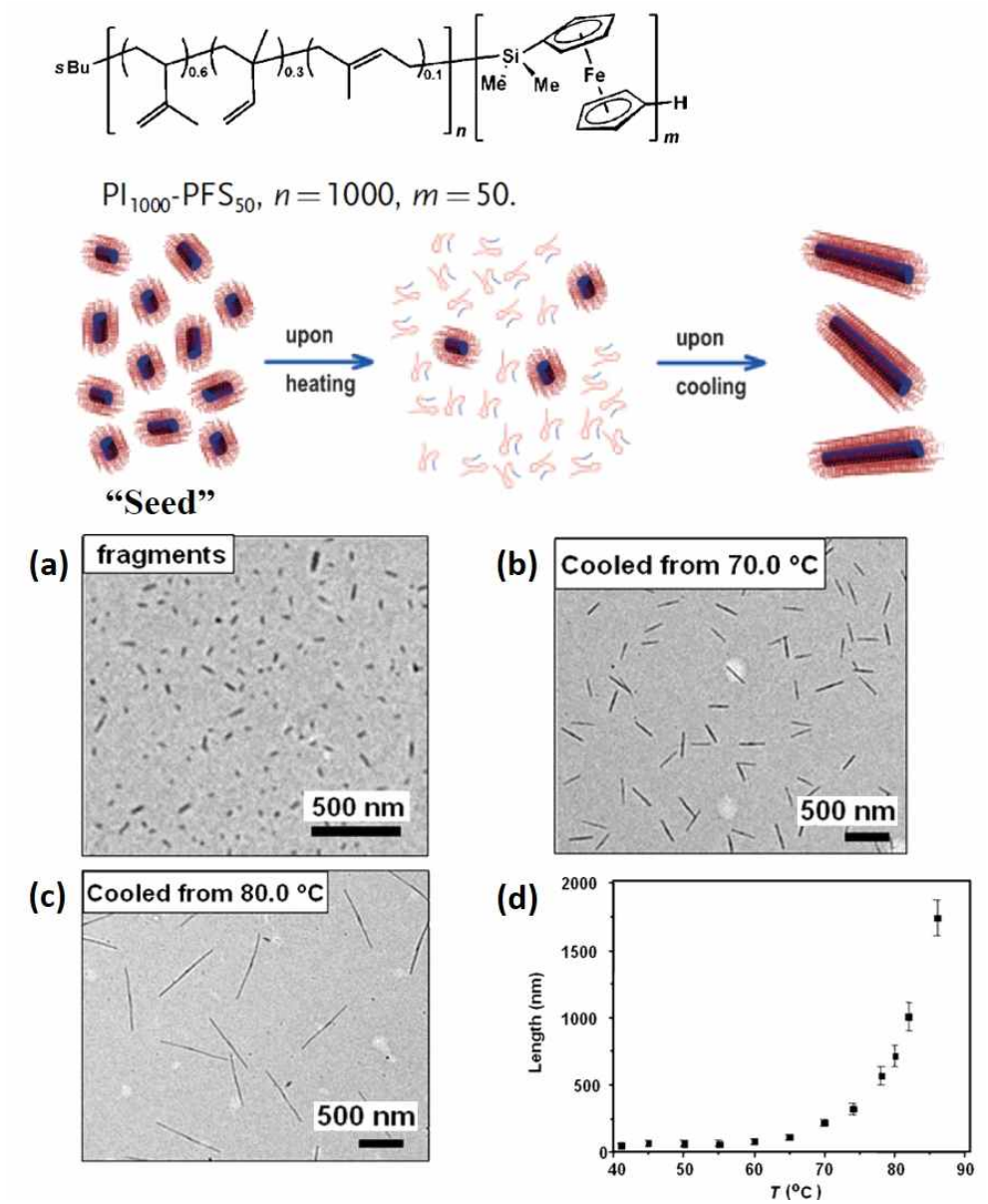

Figure 1.5. Schematic illustration of CDSA *via* self-seeding of PI_{1000}-*b*-PFS_{50} block copolymers in decane 0.1 mg/mL[27]. (a-c) TEM images of the nanofibers by self-seeding from 40 ℃ to 86 ℃. (d) The plot of annealing temperature vs. the average length distribution of the self-seeded nanofibers.

1-3. Various Nanostructures by Self-Assembly of Peptides

There are many researches of the self-assembling behavior about peptide oligomers[28,29,30,31,32,33,34], and peptide-attached block copolymer hybrids to enhance the stability of nanostructures[35,36,37]. Because peptide oligomers have diverse functionalities and easy to make self-assembly structures. Other people used synthetic polymers with peptides because polymers can be template for the peptides and increase the stability. There are also many examples to make stimuli-responsive assemblies. For example, Parquette group found that the self-assembly process can be driven by hydrophobic $\pi-\pi$ association with the electrostatic 1,4,5,8-naphthalenetetracarboxylic acid diimide (NDI) repulsion of protonated lysine groups in water (**Figure 1.6**)[34]. They demonstrate the controlled self-assembly of simple dipeptide-NDI conjugates into well-defined 1-D nanostructures. They reasoned that the hydrogen-bonding along the peptide backbone and $\pi-\pi$ association of NDI, which strongly drives β-sheet assembly in water, would be mitigated by the electrostatic repulsions of adjacent protonated lysines, resulting in soluble, well-ordered nanostructures.

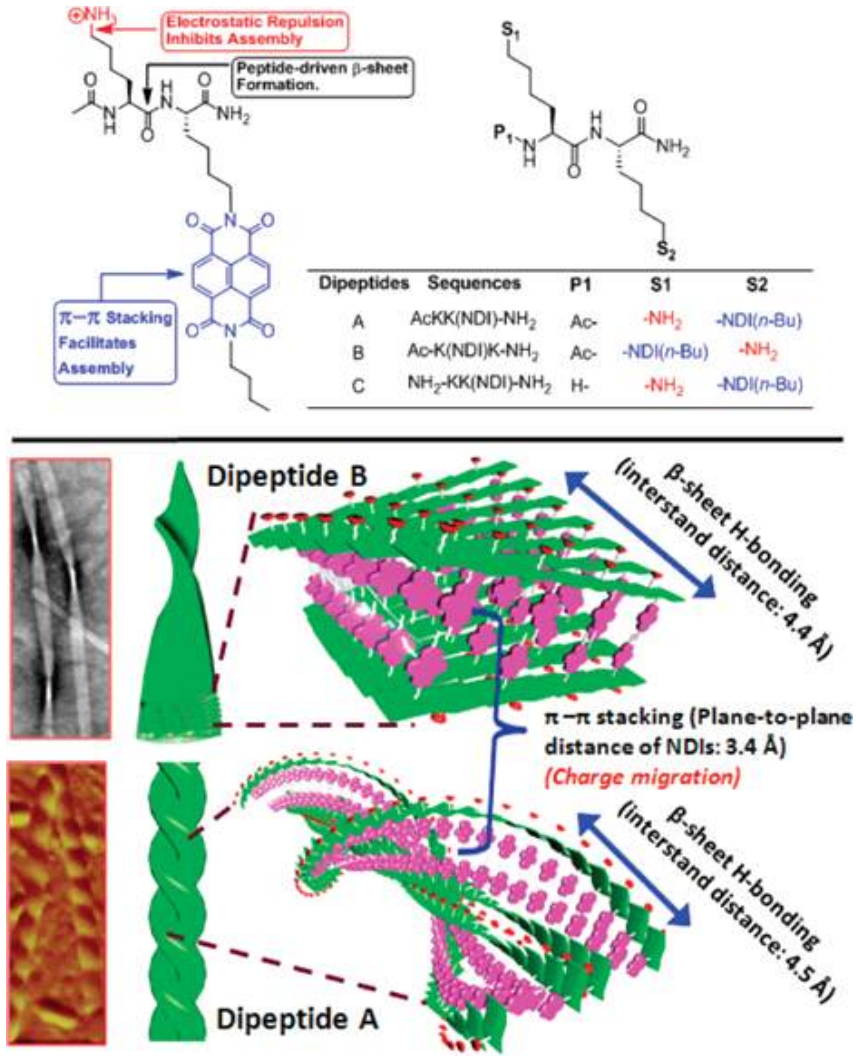

Figure 1.6. Schematic illustration of peptide dimers *via* hydrophobic $\pi-\pi$ association of NDI and electrostatic repulsion of lysines. Different peptide sequence resulted in different twisted 1D nanoribbons in water.

1-4. References

(1) Meijer, E. W. *Science*, 1995, *268*, 1592.
(2) Eisenberg, A. *Science*, 1995, *268*, 1728.
(3) Eisenberg, A. *Chem. Soc. Rev.* 2012, *41*, 5969.
(4) Eisenberg, A. *Can. J. Chem.* 1999, *77*, 1311.
(5) Park, S.-J. *J. Am. Chem. Soc.* 2011, *133*, 1517.
(6) Nandan, B. *J. Mater. Chem.* 2012, *22*, 25102.
(7) Park, S.-J. *Macromolecules*, 2014, *47*, 3720.
(8) Zhang, J. *Macromol. Rapid Commun.* 2018, *39*, 1800125.
(9) Jiang, X. *Macromolecules*, 2014, *47*, 4761.
(10) Choi, T.-L. *J. Am. Chem. Soc.* 2013, *135*, 17695.
(11) Choi, T.-L. *J. Am. Chem. Soc.* 2018, *140*, 475.
(12) Pochan, D. J. *Science*, 2007, *317*, 647.
(13) Manners, I. *ACS Nano*, 2017, *11*, 9162.
(14) Wooley, K. L. *J. Am. Chem. Soc.* 2011, *133*, 1228.
(15) Mai, Y. *Macromolecules*, 2018, *51*, 161.
(16) Wooley, K. L. *Proc. Natl. Acad. Sci. U.S.A.* 2002, *99*, 5058.
(17) Armes, S. P. *J. Am. Chem. Soc.* 2014, *136*, 10174.
(18) Choi, T.-L. *Chem. Commun.* 2014, *50*, 7945.
(19) Choi, T.-L. *J. Am. Chem. Soc.* 2012, *134*, 14291.
(20) Ihn, K. J. J. *Polym. Sci. Part B. Polym. Phys.* 1993, *31*, 735.
(21) Manners, I. *Nat. Chem.* 2010, *2*, 566.
(22) O'Reilly, R. K. *J. Am. Chem. Soc.* 2017, *139*, 16980.
(23) Manners, I. *Science*, 2018, *360*, 897.
(24) O'Reilly, R. K. *Chem. Sci.* 2011, *2*, 955.
(25) Huang, X. *Macromolecules*, 2018, *51*, 2065.
(26) Xu, J. *Nat. Mater.* 2009, *8*, 348.
(27) Manners, I. *Angew. Chem. Int. Ed.* 2011, *50*, 1622.
(28) M. Lee, *Angew. Chem. Int. Ed.,* 2007, *46*, 3475-78.

(29) M. Lee, *Angew. Chem. Int. Ed.*, 2007, 46, 9011-14.
(30) S. I. Stupp, *Nano Lett.*, 2009, *9*, 945-51.
(31) M. Lee, *Angew. Chem. Int. Ed.* 2009, *48,* 1601-05.
(32) J. Kopecek, *Macromol. Biosci.*, 2009, *9*, 36-44.
(33) W. Meier, *ACS Macro Letters,* 2014, *3*, 59-63.
(34) J. Parquette, *J. Am. Chem. Soc.*, 2009, *131*, 16374-76.
(35) H. Schlaad, *Angew. Chem. Int. Ed.,* 2006, *45*, 7578-81.
(36) H. G. Borner, *Soft Matter,* 2007, *3*, 394-408.
(37) N. Higashi, *Langmuir,* 2013, *46*, 15477-84.

Chapter 2. Control of Peptide Assembly through Directional Interactions†

†Portions of this chapter have been previously published, see: Choi, I.; Park, I.-S.; Ryu, J.-H.; Lee, M. *Chem Commun.* 2012, *48*, 8481.

Abstract

We demonstrate the self-assembly of tripeptide amphiphiles into spherical hollow capsules from linear nanoribbons *via* control of the molecular packing. We achieved a transition of arrangement from anisotropic to isotropic by an elaborate design of the molecular architecture.

Introduction

The self-assembly of peptide amphiphiles into well-organized nanostructures has been the subject of intense study due to the fundamental importance of understanding the natural peptide assembly and their potential applications.[1] Synthetic peptide amphiphiles have adopted secondary structures like α-helices and β-sheets, and further organized into more complicated nanostructures.[2,3] Recently, the construction of one-dimensional (1D) structures from short peptides such as di- or tripeptide molecules has attracted considerable attention because of their simple synthetic procedure and well-defined nanostructures with potential applications and practical implications.[4] Such nanostructures include nanoribbons, twisted ribbons, and nanotubes obtained from the self-assembly of simple peptides.[5] Such peptides usually consist of three main segments: (i) a hydrophobic group, commonly a side chain of an amino acid, such as phenylalanine and tryptophan, or aromatic segments that drive aggregation through hydrophobic and $\pi-\pi$ interaction; (ii) a β-sheet-forming peptide backbone that promotes 1-D nanofiber structures; (iii) a hydrophilic group either at the N or C terminal of the peptide amphiphiles or in the side chain of an amino acid (i.e. lysine or glutamic acid) that provides charge repulsion to prevent undefined agglomeration but instead promotes well-defined nanostructures.[6] In small peptide systems, the formation of β-sheet structures is the main driving force for assembly, and 1-D nanostructures are commonly observed due to the directional ordering derived from β-sheet hydrogen bonding. Thus, tuning of β-sheet characteristics by modifying the molecular architecture will be a rational strategy for the control of aqueous nanostructures.

Results and Discussion

For this reason, we designed three tripeptides based on lysine, where the middle lysine is functionalized with pyrene at its ε-position acting as a hydrophobic unit. The N-termini differ and are hydrogen, acetyl and Fmoc (fluorenyl-9-methoxycarbonyl), respectively (**Fig. 1**). Our key strategy to tune β-sheet characteristics is this variation of the N-terminal, as self-assembly of these tripeptides requires a delicate balance between electrostatic repulsion (here: lysine ammonium side-chains), hydrogen bonding (stabilized by hydrophobic N-termini), and hydrophobic $\pi-\pi$ interactions induced by the pyrene units. Herein, we present the self-assembly of these tripeptides into 0-D vesicle, 1-D twisted ribbon and 1-D flat ribbon structures by changing the molecular packing from an isotropic to an anisotropic arrangement induced by β-sheet formation (**Figure 1**).

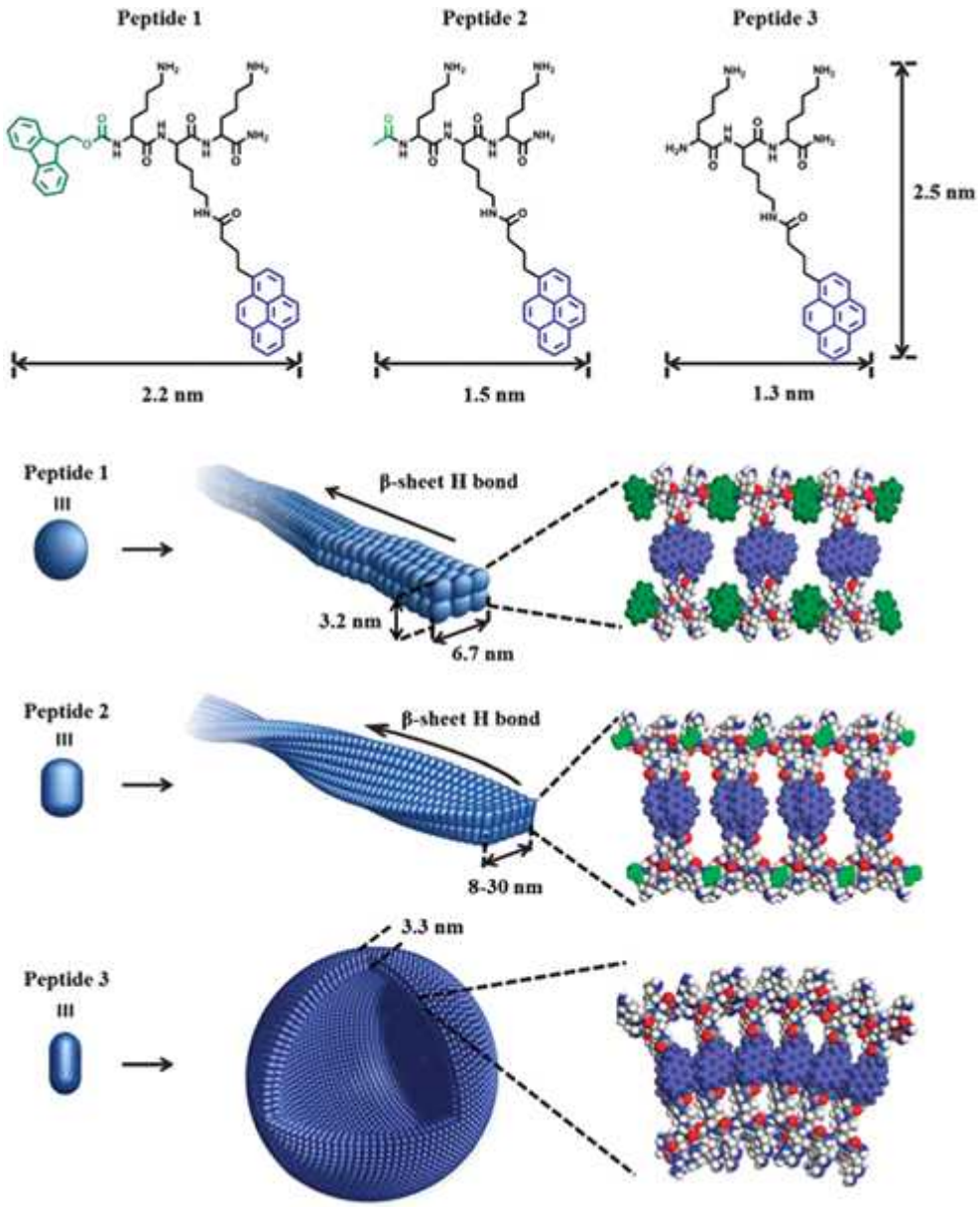

Figure 1. Molecular structures of the tripeptides and schematic presentation of their self-assembled nanostructures. Peptide 1 which has similar height and width aggregates into a flat ribbon. Peptide 2 which can be described by rectangular shape forms a twisted ribbon. Peptide 3 which has a more narrow width assembles into a vesicle structure.

Transmission electron microscopy (TEM) image of tripeptide **1** functionalized with Fmoc at the N-terminal revealed the formation of fibers with uniform diameters of 6.7 nm and lengths reaching the micrometer-scale (**Figure 2a**). Atomic force microscopy (AFM) images of tripeptide **1** confirmed that this fibril is of a flat ribbon like structure with an average height of 3.2 nm (**Figure S3, SI**). In contrast, tripeptide 2 functionalized with an acetyl group at the N-terminal formed twisted nanoribbons with sizes of 8-30 nm in width and several hundred nanometers in length (**Figure 2b**). Interestingly, tripeptide **3** showed a spherical shaped aggregation in TEM with a radius of about 40 nm (**Figure 2c**). Considering the distance between the hydrophilic amine at the ε-position of lysine and the pyrene units in **3** to be 2.5 nm, the dimension of the spheres exceeds the extended molecular length by a factor of about 16, which strongly suggests that the objects might be vesicles rather than simple micelles. In addition, the concaveness which is observed in the negatively stained TEM image indicates the shape of shrunk spheres formed during the drying process, providing further evidence of the hollow nature of the vesicular structures (**Figure 2c**). To further corroborate the formation of vesicles, we performed a cryo-TEM investigation. As shown in **Figure 2d** and **Figure S8**, the micrograph shows hollow spherical objects with a uniform wall thickness of 3.3 nm, which is slightly less than twice the extended molecular length, suggesting an interdigitated bilayer molecular packing of tripeptide **3** (**Figure 1**).

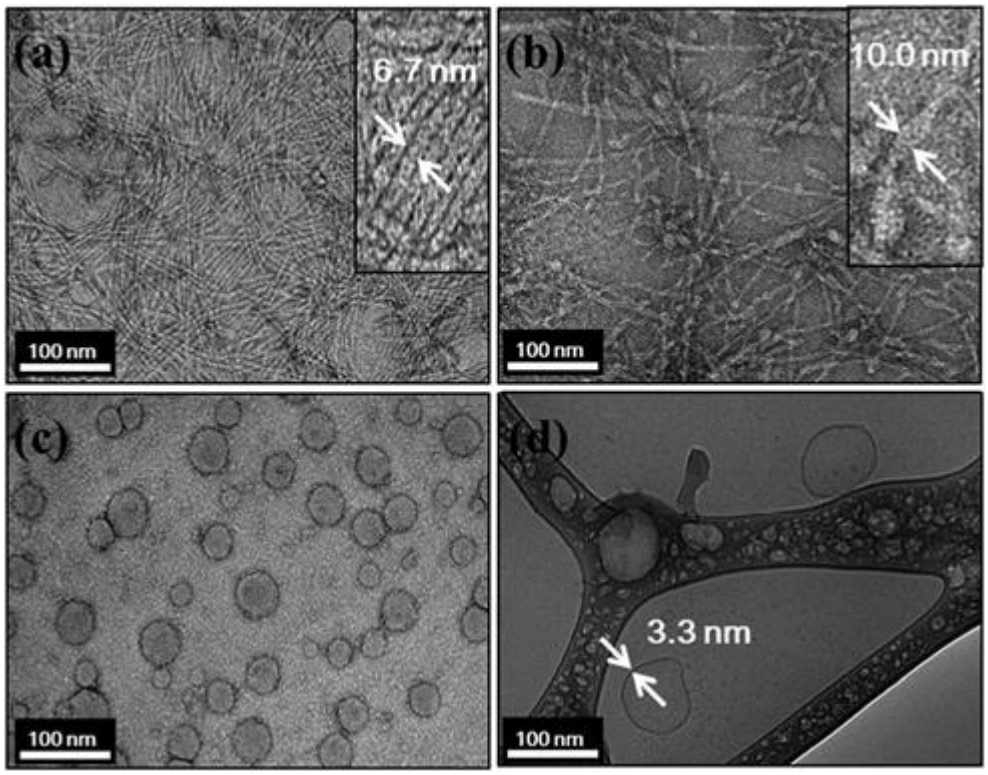

Figure 2. Negatively stained TEM images in water at 200 mM. (a) Tripeptide **1**, (b) **2**, (c) **3** and insets are magnified images of (a) and (b). (d) Cryo-TEM images of tripeptide **3** (5 mM aqueous solution).

The self-assembling behavior of the tripeptides was further scrutinized by fluorescence spectroscopy and dynamic light scattering (DLS) experiments. The absorption maxima of tripeptides **1** and **2** in aqueous solution are red-shifted and the intensities decreased with respect to the monomers in acetonitrile. This absorption behavior and the observed quenching of fluorescence indicate J-type aggregation of the pyrene segments within the ribbon structure (**Figure S4** and **S5**).[7]

Remarkably, the fluorescence of tripeptide **3** only showed the excimer peak at longer wavelength regions in water, which is an indication of inter-pyrene electronic communication between closely packed pyrene units in the excited state (**Figure 3a**).[8] DLS experiments of **3** showed a monomodal size distribution with an average hydrodynamic radius (R_H) of 40 nm (**Figure 3b**). In comparison, tripeptides **1** and **2** showed bimodal distributions and hydrodynamic radii much larger than that of **3**. These results correlate with the TEM data. Fourier-transform infrared (FTIR) spectroscopy and circular dichroism (CD) studies were applied to determine the secondary structure within the self-assembled nanostructures.[9] As shown in **Figure 3c**, the FTIR spectrum of tripeptide **1** shows a strong band at 1625 cm^{-1} and a weak signal at 1675 cm^{-1}, which are typical signals of antiparallel β-strands.[10] In contrast, tripeptide **2** showed a broad peak at 1633 cm^{-1}, indicative of the weak β-sheet hydrogen boding within the twisted ribbon. Tripeptide **3** showed a strong peak at 1672 cm^{-1} which is assigned to the trifluoroacetate counterions of the ammonium group in lysine units.[11] This indicates that tripeptide **3** adopts a random coil structure between the peptide backbone, as revealed by the lack of the characteristic peaks of hydrogen bonding in the FTIR spectrum. The CD spectrum of tripeptide **1** showed pronounced negative Cotton effects in water, while **2** and **3** displayed flat signals. This indicates that Fmoc-containing tripeptide **1** assembles into highly oriented chiral structures in water *via* strong β-sheet formation (**Figure 3d**).

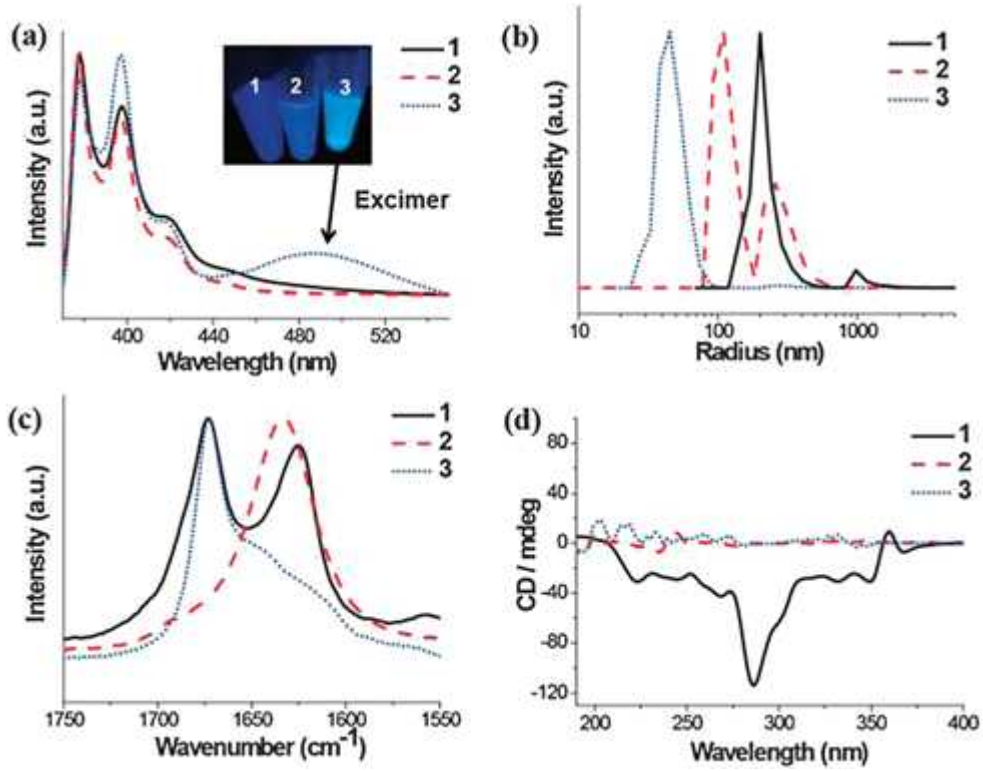

Figure 3. (a) Fluorescence spectrum (λ_{ex}= 340 nm) of tripeptides in aqueous solution at 1 mM. Only **3** shows the excimer peak at 490 nm. Inset: 1 mM aqueous solutions of **1** (left), **2** (middle), **3** (right) illuminated by a UV (365 nm) lamp. (b) R_H distribution of peptides obtained by DLS (200 mM aqueous solutions). (c) FTIR spectra of peptides in D_2O at 1 mM. (d) CD analysis of peptide secondary structures (1 mM aqueous solution) **1** (solid), **2** (dashed) and **3** (dotted).

We propose a packing model for the self-assembly of the tripeptides as shown in **Figure 1**. In the case of tripeptide **1**, the 6.7 nm width of the ribbon structure fits well with the length of three pairs of stacked β-sheets in an antiparallel packing fashion (the length of one fully extended monomeric unit was determined to be 2.2 nm from molecular modeling). Furthermore, the 3.2 nm height of the nanoribbon determined by AFM is comparable to the calculated height of an interdigitated β-sheet bilayer stack, presumably driven by hydrophobic and $\pi - \pi$ stacking interactions of overlapped pyrene units (**Figure 1**). The nanoribbons are composed of a hydrophobic pyrene interior in the bilayer β-sheet peptide domains, and a hydrophilic exterior consisting of the side chain of two lysines facing the aqueous interface. The β-sheet structure might be further stabilized by intermolecular $\pi - \pi$ interaction between the fluorenyl groups of neighboring antiparallel β-sheets. The decreasing hydrophobicity of the N-terminal group from Fmoc to acetyl induced a morphological transition from a long flat ribbon to a short twisted ribbon. This is because of a loss of $\pi - \pi$ interactions between neighboring antiparallel β-sheets, which results in a destabilization of the β-sheet and a premature termination of ribbon growth. The resulting decreased interaction between β-sheets causes weak directional ordering along the peptide backbone, resulting in the increase in width and formation of a twisted structure rather than a laterally finite flattened ribbon. The removal of the hydrophobic group from the N-terminal changes the molecular packing from an anisotropic conformation to an isotropic one. Tripeptides **1** and **2** show directional order forming β-sheets induced by the hydrophobic interactions at N-termini, resulting in a 1-D nanoribbon structure. In the case of peptide **3**, the absence of the hydrophobic interactions at N-termini increases the flexibility of the

molecular arrangement, which provides the possibility of forming curvature. Also, by the flexibility of the molecular arrangement, peptide **3** can make a denser packing structure with a face-to-face overlapping of interpyrene units resulting in excimer formation. These results suggest that tripeptide **3** adopts an isotropic planar conformation rather than the directional ordered anisotropic conformation like **1** and **2**, leading to hollow vesicular structures.

Conclusion

In conclusion, we reported the rational design of tripeptide amphiphiles for the formation of 0-D and 1-D nanostructures and explained the self-assembling behavior based on their molecular architecture. Tripeptide **1** forms 1-D flat ribbons through an anisotropic arrangement of peptides by strong β-sheet formation stabilized with intermolecular fluorenyl $\pi-\pi$ interaction at the N-terminal Fmoc. Peptide **2** with acetyl as a smaller hydrophobic N-terminal, aggregates into a twisted ribbon structure due to weaker β-sheet formation. The removal of the hydrophobic group from the N-terminal induces an isotropic molecular packing, resulting in 0-D spherical nanocapsules. The results here imply that a delicate balance between β-sheet formation and hydrophobic $\pi-\pi$ interaction plays a critical role in the self-assembly of short peptide amphiphiles. We believe that this fundamental understanding of peptide self-assembly will provide an important strategy to design well-defined nanostructures using small peptide building blocks for advanced nano- and biomaterials.

Experimental Section

Materials and techniques

1-Pyrenebutyric acid *N*-hydroxysuccinimide ester (95%) from Aldrich, Fmoc-Lys(Boc)-OH (98%) from Aldrich and Trifluoroacetic acid (99%) from Aldrich were used as received. Rink amide MBHA resin (100-200 mesh) from Beadtech, 2-(1H-Benzotriazole-1-yl)-1,1,3,3 -tetramethyluronium hexafluorophosphate (HBTU) from Beadtech, Diisopropylethylamine (DIPEA) (99%) from Aldrich, acetic anhydride (99%) from Aldrich were used as received.

All atmosphere sensitive reactions were done under argon. Flash chromatography was carried out with Silica Gel 60(230-400 mesh) from EM science. Visualization was accompanied with UV light and iodine vapor. ^{1}H-NMR spectra were recorded from DMSO-d_6 on a Bruker AM 300 spectrometer. The purity of the products was checked by thin layer chromatography (TLC; Merck, silicagel 60). MALDI-TOF-MS was performed on a Perseptive Biosystems Voyager-DE STR using α-Cyano-4-hydroxycinnamic acid matrix. Preparative high performance liquid chromatography (HPLC) was performed at room temperature using a 20 mm × 600 mm poly styrene column on a Japan Analytical Industry Model LC-908 recycling preparative HPLC system, equipped with UV detector 310 and RI detector RI-5. Dynamic light scattering (DLS) were performed with an ALV/CGS-3 Compact Goniometer System. The fluorescence spectra were measured in a Hitachi F-4500 fluorescence spectrophotometer. The transmission electron microscopy (TEM) was performed at 120 kV using JEM-2010. The atomic force microscopy (AFM) was performed with a Bruker Nanoscope V Multimode 8 instrument.

Circular dichroism

CD spectra were measured using a JASCO model J-810 spectropolarimeter equipped with temperature controller. Spectra were recorded from 500 nm to 190 nm using a 0.1 cm path-length cuvette. Scans were repeated five times and averaged. Molar ellipticity was calculated per amino acid residue. Peptide concentration was 200 μM. Sample solutions were incubated at least for 3 days before measurement, and essentially the same CD spectra were obtained after prolonged incubation, indicating thermodynamic equilibrium states.

Fourier Transform Infrared (FTIR) Spectroscopy

All FTIR spectra were collected on a Nicolet FTIR spectrometer at ambient temperature. The instrument was continuously purged with CO_2-free dry air. Interferograms were recorded between 1700 and 1600 cm^{-1} at are solution of 4 cm^{-1}, and a total of 256 scans were averaged. Samples for FTIR were dissolved in D_2O (about 10 mg/mL) and analyzed in a transmission cell having CaF_2 windows and a 0.025 μm path length.

Dynamic light scattering (DLS)

DLS experiment was performed at room temperature with LV/CGS-3 Compact Goniometer System equipped with He-Ne laser operating at 632.8 nm. The scattering angle was 90° . Before measurement, the sample was centrifuged at 10,000 × g for 20 min to sediment any dust particles. Sample concentrations were typically 200 μM in water. The size distribution was determined by using a constrained regularization method. The hydrodynamic radius (R_H) was determined from the DLS auto correlation functions by the cumulants and the CONTIN methods using the software provided by the manufacturer.

Atomic Force Microscopy (AFM)

The AFM images were collected on a NanoScope V device at ambient temperature in tapping mode using silicon tips (NSC14/AIBS, MikroMasch). 10 μL of the sample solution (200 μM) was used and then was place on freshly cleaved silicon wafer. Adsorb sample for 1 day under dry conditions. The resultant substrates were rinsed with solvent (50 μL) twice to remove the loosely bound peptide and the samples were stored in a desiccator *in vacuo* for 1 h before imaging. The scanning speed was at a line frequency of 1.0 Hz, and the original images were sampled at a resolution of 512 x 512 pixels.

Transmission electron microscopy (TEM)

Transmission electron microscopy observation was carried out with a JEOL JEM-2010 operated at 120 kV. For study of structure of laterally-grafted amphiphilic molecules in aqueous solution, a drop of aqueous solution (0.01 %) was placed on a carbon-coated copper grid and allowing the solution to evaporate under ambient conditions.

The cryogenic transmission electron microscopy experiments (cryo-TEM) were performed with a thin film of aqueous solution of molecule (5 μL) transferred to a lacey supported grid. The thin aqueous films were prepared under controlled temperature and humidity conditions (97-99%) within a custom-built environmental chamber in order to prevent evaporation of water from sample solution. The excess liquid was blotted with filter paper for 2-3 seconds, and the thin aqueous films were rapidly vitrified by plunging them into liquid ethane (cooled by liquid nitrogen) at its freezing point. To investigate the effect of temperature, solution were sealed with Teflon tape and elevated the desired temperature in Daehan Scientific precision digital refrigerated circulator having an accuracy ± 0.1 ℃. The system was maintained for 1 h. And then solution was placed on the lacey supported grid, and

thin aqueous films were quickly quenched in liquid ethane. The grid was transferred, on a Gatan 626 cryo holder, using a cryo transfer device. After that they were transferred to a JEM-2010 TEM. Direct imaging was carried out at a temperature of approximately -175 ℃ and with a 120 kV accelerating voltage, using the images acquired with a Dual vision 300W and SC 1000 CCD camera (Gatan, Inc; Warrendale, PA)

X-ray diffraction (XRD)

Data was collected on an X-ray scattering 5D beamline in Pohang Accelerator Laboratory with a wavelength of 1.23984 Å. By varying the scattering angle the explored momentum transfer vector (q) was in the range of $5.3 < q\ (\mathrm{nm}^{-1}) < 18.3$, with $q = 4\pi \sin\theta / \lambda$, where θ is the scattering angle. The tripeptides at 5 mg/mL was spread on a silicon wafer slide as a film and allowed to air dry prior to data collection.

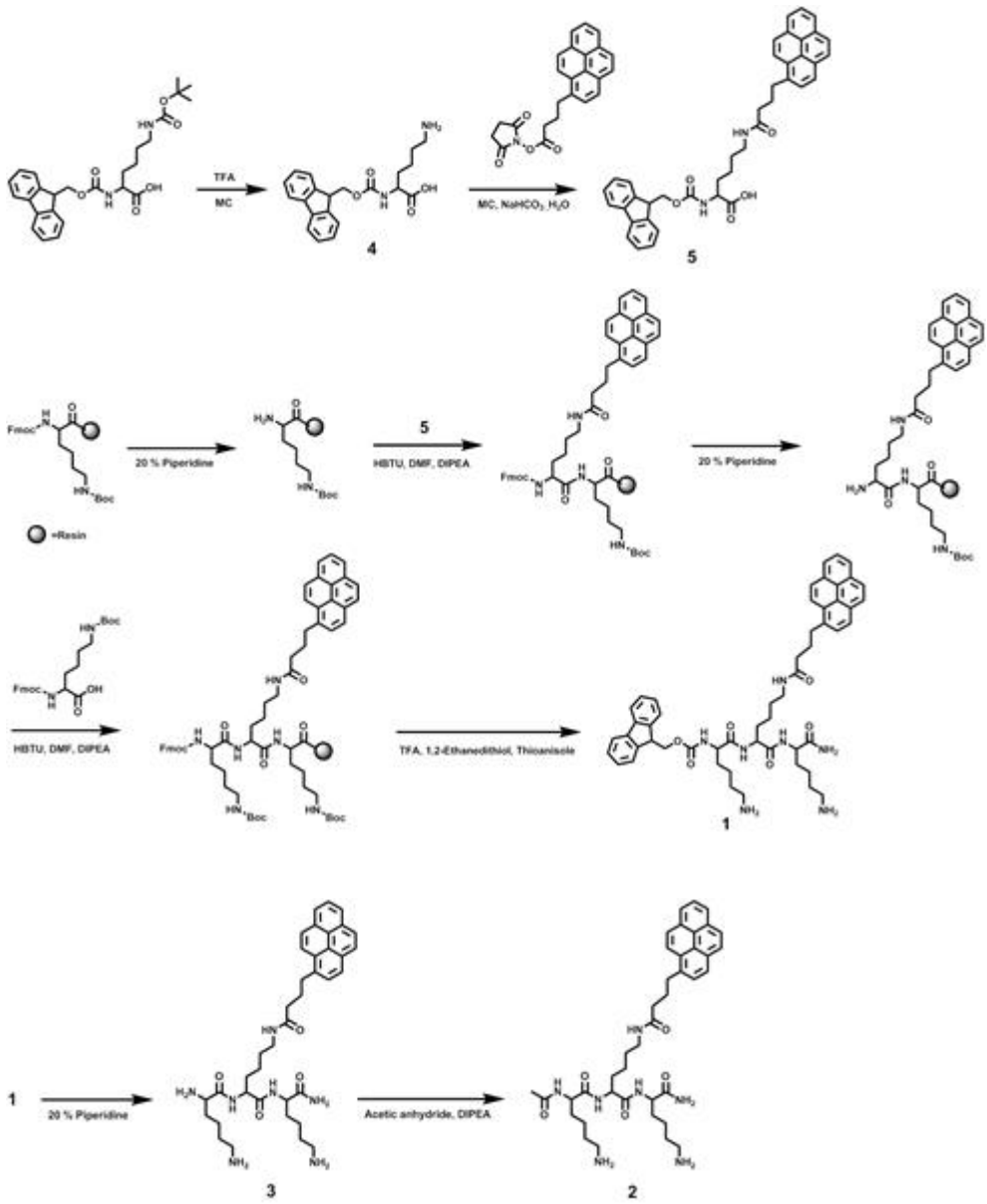

Scheme 1. Synthesis of compounds 1, 2 and 3.

Synthesis of compound 4

Fmoc-Lys(Boc)-OH (853.68 mg, 1.822 mmol) were dissolved in methylene chloride (50 mL). Trifluoroacetic acid (0.383 mL, 5 mmol) was added to the solution. The reaction mixture was stirred over 2 h under argon. The purity of the products was checked by thin layer chromatography. It was used for next reaction without further purification.

Synthesis of compound 5

To a solution of compound **4** in methylene chloride (100 mL) was dropped in 1-Pyrenebutyric acid *N*-hydroxysuccinimide ester (668.3 mg, 1.734 mmol) dissolved in methylene chloride (50mL). Degassed 2 M aqueous $NaHCO_3$ (50 mL) was added to the solution. The mixture was the aqueous layer was washed twice with ethyl acetate. The combined organic layer was dried over anhydrous magnesium sulfate and filtered. The solvent was removed in a rotary evaporator, and the crude product was purified by column chromatography (silica gel) using ethyl acetate/hexane as eluent to yield 730 mg (88%) of brown solid. ^{1}H-NMR (300 MHz, DMSO-d_6, ppm): δ =11.0 (s, 1H; carboxylic acid-*H*), 8.12-7.71 (m, 9H; phenanthrene-*H*), 8.03 (s, 2H; sec. amide-*H*), 7.87-4.46 (m, 9H; fluoren-*H*), 4.70-1.25 (m, 16H; methylene-*H*), 4.55 (m, 1H; methane-*H*)

Synthesis of compound 1, 2, and 3

Peptide was synthesized on Rink amide MBHA resin using standard Fmoc protocols on a microwave peptide synthesizer. Before addition to the resin, a mixture of HBTU (20.48 mg, 54 μmol), dimethylformamide (DMF) (1 mL), and 1% diisopropylethylamine (DIPEA) (21 μL, 120 μmol) and amino acids was incubated for 10 min for carboxyl activation. The amino acid groups were employed,

Fmoc-Lys(Boc)-OH and compound **5** (Fmoc-Lys (Pyrene)-OH. For deprotection of the Fmoc group from the resin, the resin was treated with 20% piperidine in DMF (3 mL) and microwave turned on for Fmoc deprotecting. Then the resin was washed successively with DMF and methylene chloride. Next, the mixture of Fmoc-Lys(Boc)-OH and DMF (3 mL) were added to the resin and microwave turned on for peptide coupling. Repeat this procedure of deprotecting, coupling and deprotecting, for three times, peptide synthesis ended. For synthesis of peptide **2**, acetic anhydride (3 mL) and DIPEA (21 μL, 120 μmol) added to last product of deprotected peptide. For synthesis of peptide **1**, last process of Fmoc deprotecting was not needed. And the resin was precipitated by THF, and dried *in vacuo*. The dried resin was treated with cleavage cocktail (TFA: 1,2-ethanedithiol: thioanisole; 95 : 2.5 : 2.5) for 3 h, and was triturated with hexane and *tert*-butyl methyl ether (5 mL each). The peptides were purified by reverse-phase HPLC eluting with a linear gradient of acetonitrile/water (35/65 to 100/0 over 30 minutes, 0.1% TFA). The molecular weight was confirmed by MALDI-TOF mass spectrometry. The purity of the peptides was > 95% as determined by analytical HPLC. Concentration was determined spectrophotometrically in water using a molar extinction coefficient of pyrene (54,000 $M^{-1}cm^{-1}$) at 335 nm.

Supporting Information

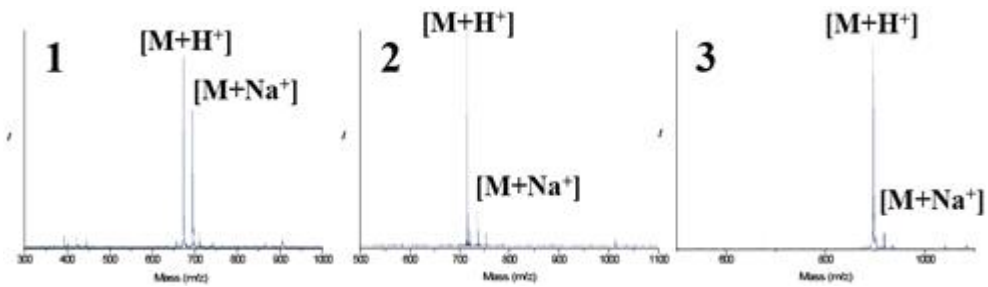

Figure S1. MALDI-TOF mass spectra of **1**, **2** and **3**. MALDI-TOF calculated mass for **1**($C_{38}H_{54}N_7O_4$ – $[M+H^+]$) is 672.42, found 673.43.
2 ($C_{40}H_{56}N_7O_5$ – $[M+H^+]$) is 713.43, found 713.93.
3 ($C_{53}H_{63}N_7O_6$ – $[M+H^+]$) is 894.48, found 895.00.

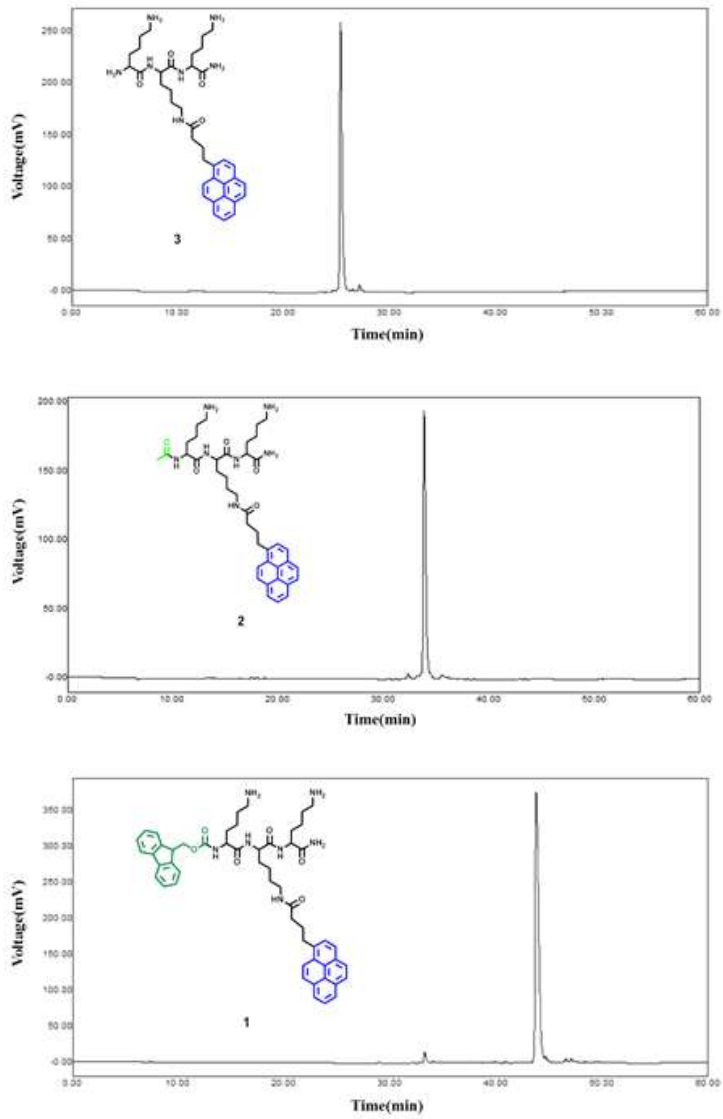

Figure S2. Analytical HPLC graph data of peptide **1**, **2** and **3**. Performed HPLC by VYDAC C18 column, eluent condition is water/acetonitrile (100:0 to 30:70 over 60 min, 0.1% TFA) and loading 20 μL each. Increasing hydrophobicity at N-termini of the peptide from **3** to **1**, the retention time also increased.

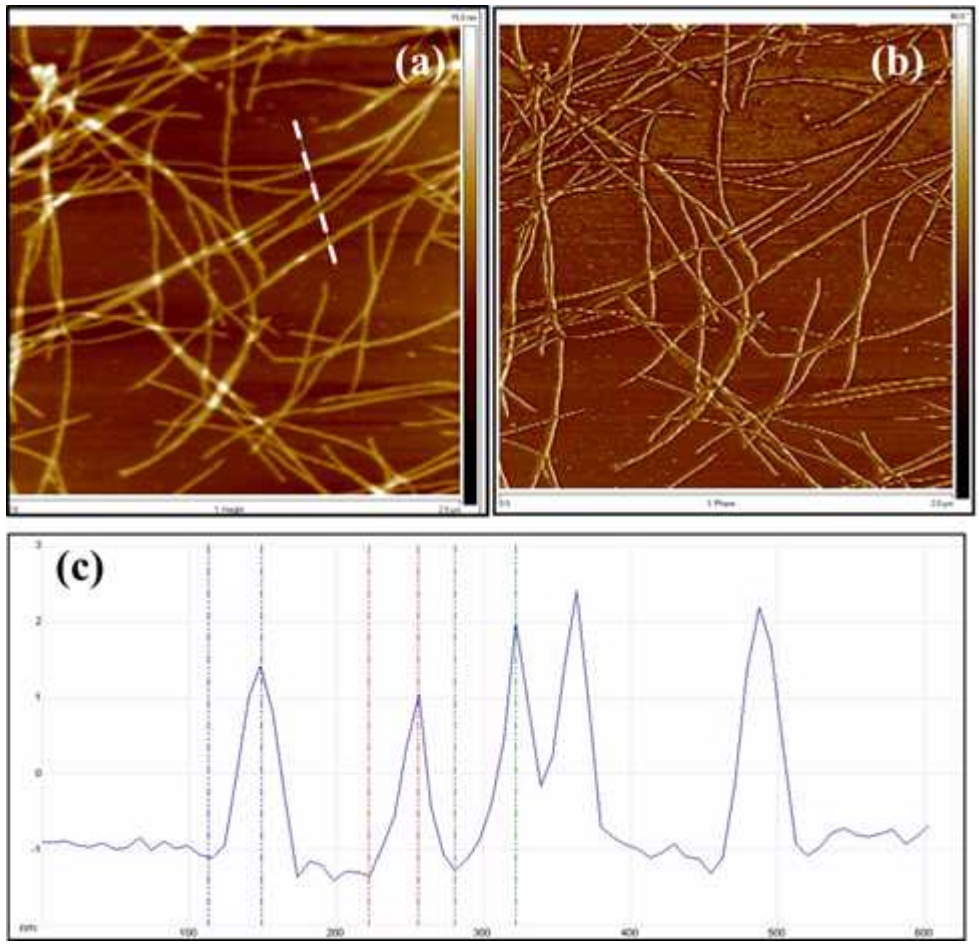

Figure S3. AFM image of tripeptide **1** with (a) height and (b) phase image at 200 μM in aqueous solution. (c) Section analysis along the line showed regular height of 3.2 nm.

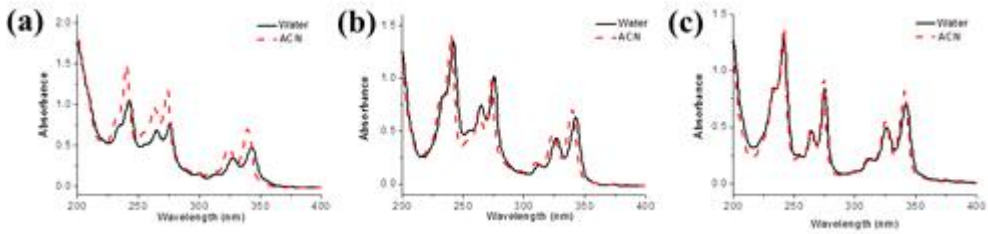

Figure S4. UV spectra of tripeptides 1(a), 2(b) and 3(c). UV absorption maxima of tripeptides in aqueous solution were red-shifted with respect to those recorded in acetonitrile which tripeptides did not assemble. It indicates *J*-type aggregation of the pyrene segments within the ribbon structure. All solutions were at 200 μM.

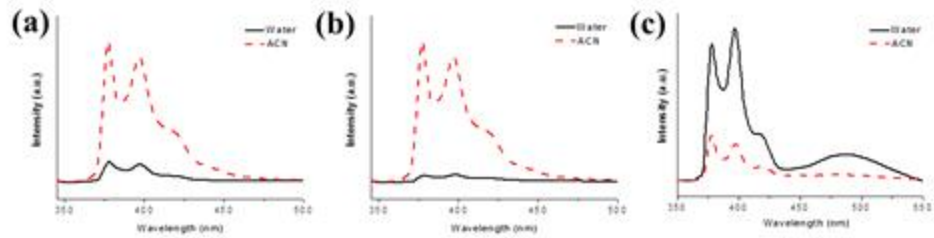

Figure S5. Changes in the emission (λ_{ex} = 340 nm) spectra of peptides, (a) 1 in aqueous solution (1 mM, solid) and 1 in acetonitrile (1 mM, dash). (b) 2 in aqueous solution (1 mM, solid) and 2 in acetonitrile (1 mM dash). The fluorescence spectra were quenched with respect to those recorded in acetonitrile, which supported UV data. But 3 had opposite tendency in emission spectrum, indicating that peptide 3 might have aggregates in organic solvent.

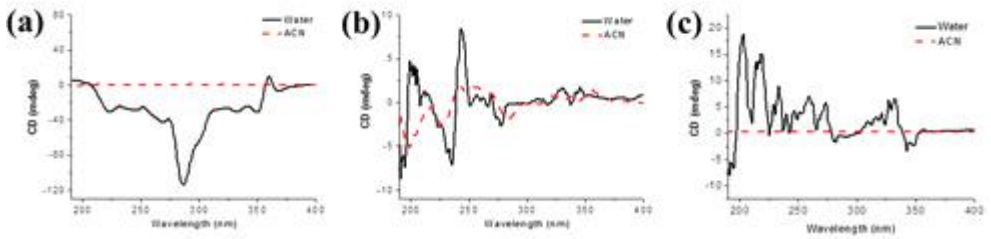

Figure S6. CD analysis of peptide secondary structures in 1 mM aqueous solution (solid) and in 1 mM acetonitrile (dash). (a) Tripeptide **1**, (b) **2** and (c) **3**. Compared to other homologue **2** and **3**, which are random structures, CD spectrum of tripeptide **1** is shown to consist predominantly of β-sheet (Figure S6a). But **1** displayed flat signals in cetonitrile, it means that secondary structures of **1** were disassembled.

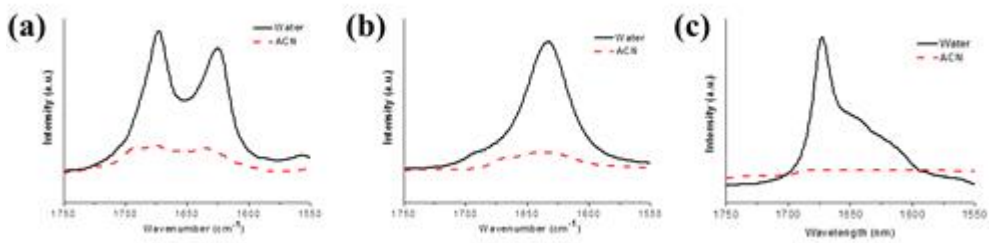

Figure S7. FT-IR spectra of tripeptides in D_2O(1 mM, solid) and in acetonitrile (1 mM, dash). (a) **1**, (b) **2** and (c) **3**. Similar with the CD spectra, FT-IR spectra of tripeptides showed flat signals in acetonitrile rather than in aqueous solutions.

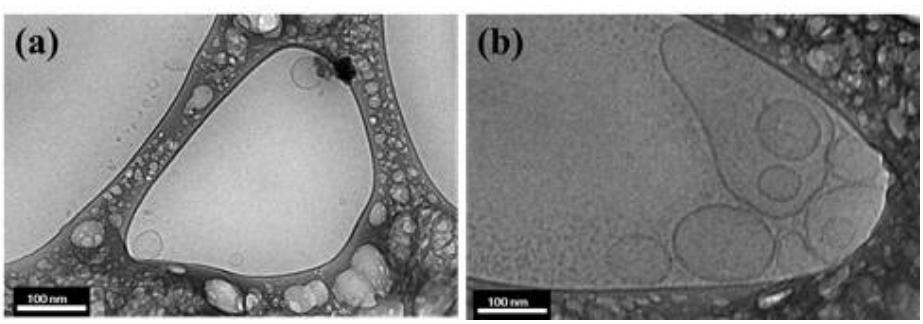

Figure S8. Cryo-TEM images of peptide **3**. The radius of the vesicles is about 20 nm to 100 nm.

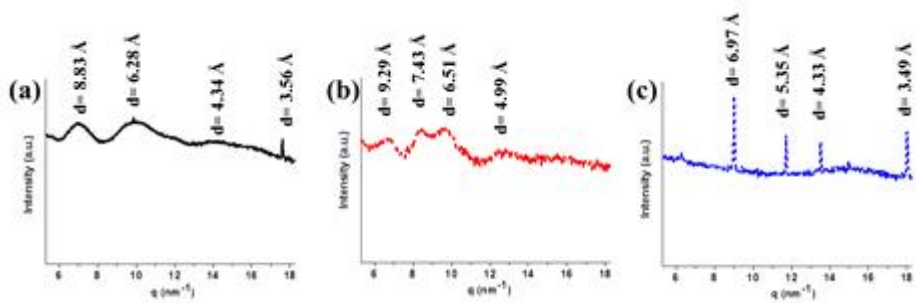

Figure S9. Wide Angle X-ray Scattering data of peptides (a) **1**, (b) **2** and (c) **3** spread as a film on a silicon wafer slide. The XRD peaks at 3.56 and 4.34 Å corresponding to the spacing between pairs of pyrene groups and the spacing of peptide within a β-sheet structure, respectively.[12] Peptide **1** and **2** show broad pattern indicating irregular packing of the aromatic segments. In contrast, **3** shows sharp XRD pattern, indicating that aromatic segments aligned with ordered structure through strong $\pi-\pi$ interactions. However, the driving forces that lead to the well-defined nanostructures are not clear at this point.

References

(1) (a) E. Gazit, *Chem. Soc. Rev.*, 2007, **36**, 1263-1269; (b) S. Zhang, *Nature Biotechnol.*, 2003, **21**, 1171-1178; (c) Y. Lim, K. S. Moon and M. Lee, *Chem. Soc. Rev.*, 2009, **38**, 925-934; (d) M. Zelzer and R. V. Ulijn, *Chem. Soc. Rev.,* 2010, **39**, 3351-3357; (e) H. Cui, M. J. Webber and S. I. Stupp, *Peptide Sci.*, 2010, **94**, 1-18.

(2) (a) V. Percec, A. E. Dulcey, V. S. K. Balagurusamy, Y. Miura, J. Smidrkal, M. Peterca, S. Nummelin, U. Edlund, S. D. Hudson, P. A. Heiney, H. Duan, S. N. Magonov and S. A. Vinogradov, *Nature*, 2004, **430**, 764-768; (b) I. W. Hamley, *Soft Matter*, 2011, **7**, 4122-4138; (c) Y. Lim, K. Moon and M. Lee, *Angew. Chem. Int. Ed.,* 2009, **48**, 1601-1605. (d) S. Scanlon and A. Aggeli, *Nano today*, 2008, **3**, 22-30; (e) X. Zhao, F. Pan, H. Xu, M. Yassen, H. Shan, C. A. E. Hauser, S. Zhang and J. R. Lu, *Chem. Soc. Rev.*, 2010, **39**, 3480-3498;

(3) (a) A. Aggeli, M. Bell, N. Boden, J. N. Keen, P. F. Knowles, T. C. B. McLeish, M. Pitkeathly and S. E. Radford, *Nature*, 1997, **386**, 259-262; (b) R. P. W. Davies, A. Aggeli, A. J. Beevers, N. Boden, L. M. Carrick, C. W. G. Fishwick, T. C. B. McLeish, I. Nyrkova and A. N. Semenov, *Supramol. Chem.*, 2006, **18**, 435-443; (c) H. Cui, T. Muraoka, A. Cheetham and S. I. Stupp, *Nano Lett.*, 2009, **9**, 945-951; (d) M. J. Krysmann, V. Castelletto, J. E. McKendrick, L. A. Clifton and I. W. Hamley, *Langmuir*, 2008, **24**, 8158-8162; (e) C. W. G. Fishwick, A. J. Beevers, L. M. Carrick, C. D. Whitehouse, A. Aggeli and N. Boden, *Nano Lett.*, 2003, **3**, 1475-1479.

(4) (a) H. Shao, J. W. Lockman and J. R. Parquette, *J. Am. Chem. Soc.*, 2007, **129**, 1884-1885. (b) Y. Lin, Y. Qiao, P. Tang, Z. Li and J. Huang, *Soft Matter*, 2011, **7**, 2762-2769; (c) N. Amdurskky, M. Molotskii, E. Gazit and G. Rosenman, *J. Am. Chem. Soc.,* 2010, **132**, 15632-15636.

(5) (a) H. Shao, T. Nguyen, N. C. Romano, D. A. Modarelli and J. R. Parquette, *J. Am. Chem. Soc.*, 2009, **131**, 16374-16376; (b) M. Reches and E. Gazit, *Phys. Biol.*, 2006, **3**, S10-S19; (c) H. Shao, J. Seifert, N. C. Romano, M. Gao, J. J. Helmus, C. P. Jaroniec, D. A. Modarelli and J. R. Parquette, *Angew. Chem. Int. Ed.*, 2010, **49**, 7688-7691; (d) H. Shao, J. R. Parquette, *Chem. Commun.*, 2010, **46**, 4285-4287.

(6) (a) M. Z. Menzenski and I. A. Banerjee, *New. J. Chem.*, 2007, **31**, 1674-1680; (b) G. Cheng, V. Castelletto, C. M. Moulton, G. E. Newby and I. W. Hamley, *Langmuir*, 2010, **26**, 4990-4998; (c) R. Orbach, L. Adler-Abramovich, S. Zigerson, I. Mironi-Harpaz, D. Seliktar and E. Gazit, *Biomacromolecules*, 2009, **10**, 2646-2651.

(7) (a) F. Wurthner. T. E. Kaiser and C. R. Saha-Moller, *Angew. Chem. Int. Ed.*, 2011, **50**, 3376-3410; (b) J. B. Birks, *Rep. Prog. Phys.*, 1975, **38**, 903-974.

(8) (a) K. H. Han, E. Lee, J. S. Kim and B. K. Cho, *J. Am. Chem. Soc.*, 2008, **130**, 13858-13859; (b) J. S. Yang, C. S. Lin and C. Y. Hwang, *Org. Lett.*, 2001, **3**, 889-892; (c) E. J. Jun, H. N. Won, J. S. Kim, K. H. Lee and J. Yoon, *Tetrahedron Lett.*, 2006, **47**, 4577-4580.

(9) (a) M. A. Bryan, J. W. Brauner, G. Anderle, C. R. Flach, B. Brodsky and R. Mendelsohn, *J. Am. Chem. Soc.*, 2007, **129**, 7877-7884; (b) J. Kong and S. Yu, *Acta Biochim. Biophys. Sin.*, 2007, **39**, 549-559; (c) S. M. Kelly and N. C. Price, *Curr. Protein Pept. Sci.*, 2000, **1**, 349-384.

(10) (a) R. Khurana and A. L. Fink, *Biophys. J.*, 2000, **78**, 994-1000; (b) P. Kupser, K. Pagel, J. Oomens, N. C. Polfer, B. Koksch, G. Meijer and G. von Helden, *J. Am. Chem. Soc.*, 2010, **132**, 2085-2093; (c) D. M. Kashirinn, A. V. Sibilev, V. L. Beloborodov and V. I. Deigin, *Pharm. Chem. J.*, 2000, **34**, 619-622.

(11) (a) C. J. Bowerman, W. Liyanage, A. J. Federation and B. L. Nilsson, *Biomacromolecules*, 2011, **12**, 2735-2745; (b) J. Madine, H. A. Davies, C. Shaw, I. W. Hamley and D. A. Middleton, *Chem. Commun.*, 2012, **48**, 2976-2978.

(12) A. M. Smith, R. J. Williams, C. Tang, P. Coppo, R. F. Collins, M. L. Turner, A. Saiani and R. V. Ulijn, *Adv. Mater*, 2008, **20**, 37-41.

Chapter 3. Synthesis of Block Copolymers for Hierarchical Self-Assemblies of Hybrid Nanostructures

Abstract

To generate hybrid nanostructures and their hierarchical self-assemblies, we synthesized amphiphilic diblock copolymers containing Fmoc-lysine units by the RAFT polymerization. The peptide-functionalized diblock copolymers were organized into layered vesicles in aqueous solutions. In addition, triblock copolymers were synthesized to induce hierarchical self-assemblies of multi-compartment micelles, in which nanoparticles can be loaded or synthesized by incorporating them selectively in one of the blocks.

Introduction

There is an example using thermo-responsive poly *N*-isoropylacrylamide (PNIPAM) group and pH responsive group containing block copolymer[1]. By changing pH or temperature, block copolymer micelle denaturalize the blocks and then alter the roles of A and B, lead to micelle inversion.

By these reasons, we want to synthesize the block copolymers which can be manipulated their self-assembling behavior by changing environment such as pH or temperature.

Results and Discussion

Then, we synthesized the amphiphilic diblock copolymer, and the hydrophilic part of the block copolymer is poly *N*-isoropylacrylamide (PNIPAM) and hydrophobic part is poly pentafluorophenylacrylate (PPFPA). Next, we modified hydrophobic PPFPA part of the block copolymer by peptide in order to change in self-assembly structures (Figure 1). We selected Fmoc-Lys-OH peptide because Fmoc group has directional ordering property forming β-sheets. Also ε-position of the lysine N-terminal is exposed. So we can attach this amine functionalized molecule to PPFPA part.

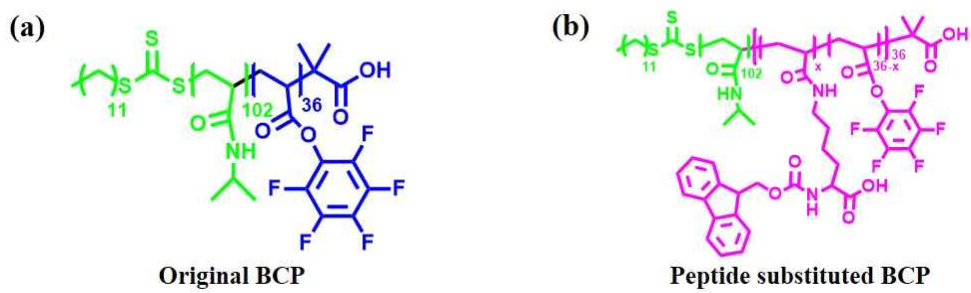

Figure 1. (a) The original PNIPAM-*b*-PPFPA diblock copolymer, (b) the peptide substituted PNIPAM-*b*-PPFPA diblock copolymer by Fmoc-Lys-OH.

At first, we checked the micelle forming condition of this block copolymer. It changed its morphology by changing solvents. In water, PNIPAM-*b*-PPFPA block copolymer makes the micelle, the corona is hydrophilic PNIPAM and the core is hydrophobic PPFPA. But in toluene, hydrophilic PNIPAM goes to core and hydrophobic PPFPA becomes corona(Figure 2). Diameter of the micelle in water is about 20 nm but reverse micelle is 10 nm in toluene. Because hydrophilic part is longer than hydrophobic part. So in water, hydrophilic PNIPAM goes

outside and micelle is bigger. After substitution, peptide-polymer hybrid shows complex morphology in aqueous solution (**Figure 3**). Its diameter is about 20 to 40 nm.

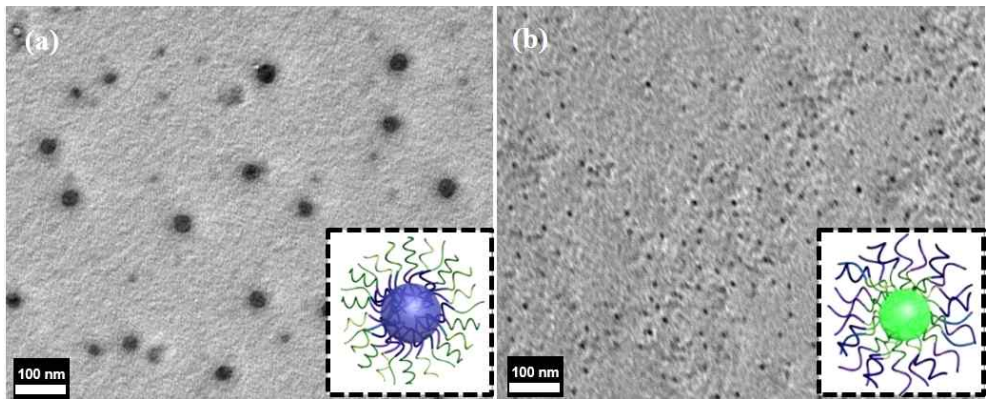

Figure 2. (a) TEM image of PNIPAM-*b*-PPFPA diblock copolymer in aqueous solution 0.5 wt.%, and (b) TEM image of PNIPAM-*b*-PPFPA diblock copolymer in toluene 0.5 wt.%.

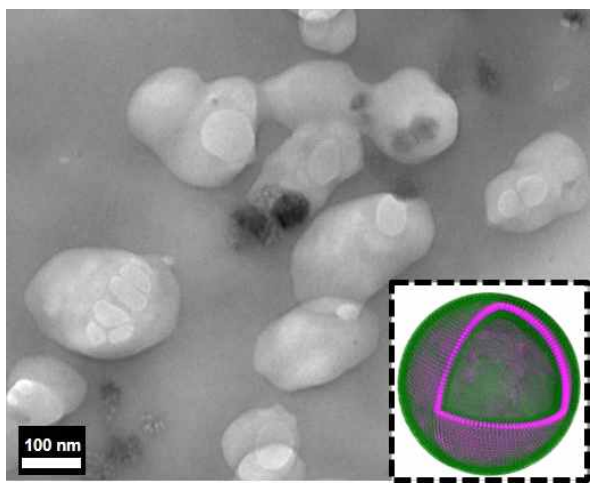

Figure 3. TEM image of peptide substituted diblock copolymer in aqueous solution 0.5 wt.%

Conclusion

We demonstrated the water-soluble diblock copolymers containing thermoresponsive PNIPAM block and modifiable PPFPA and introduced peptide units to change the self-assembled nanostructures. The original diblock copolymer made well-controlled micelles in aqueous solution, and the micelle changed its corona and core in toluene. The substitution of PPFPA block with peptide showed dramatic change of its nanostructures to vesicle structures, which could be used in drug delivery system.

Experimental Section

Materials

Without additional notes, all reagents were commercially available from Sigma-Aldrich®, Tokyo Chemical Industry Co. Ltd., and Alfa Aesar®, and were used without further purification.

General analytical information

NMR spectra were recorded by Varian/Oxford As-500 (500 MHz for ^{1}H and 125 MHz for ^{19}F) spectrometers.

Transmission electron microscopy

TEM imaging was performed using JEM-2100 (JEOL) at 120 kV. The samples were prepared by drop casting one drop of the polymer solution (10 μL) on the Formvar and carbon-coated copper grid.

Experimental Procedure for Diblock Copolymer Preparation

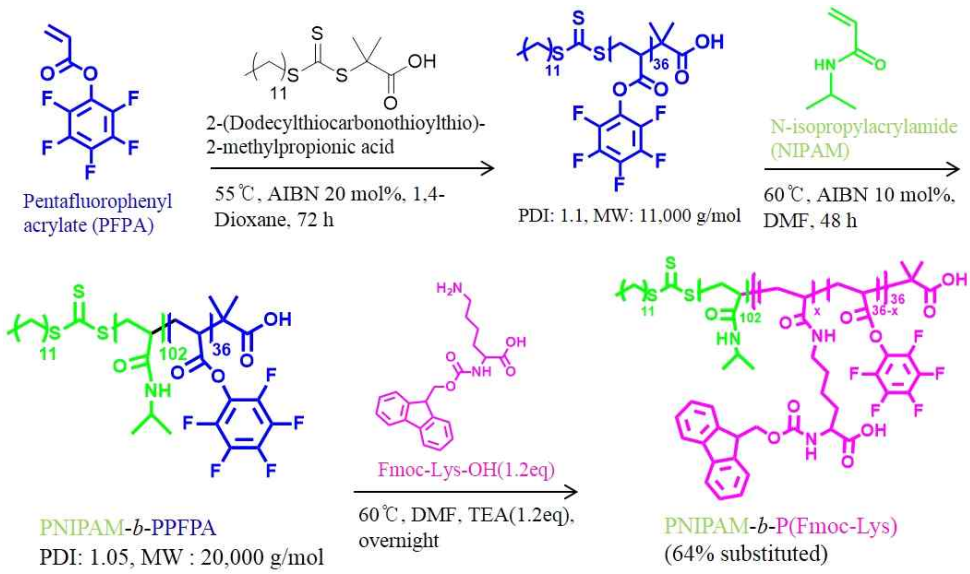

Pentafluorophenyl acrylate (PFPA), chain transfer agent, and AIBN were dissolved in 1,4-dioxane and freeze-thaw four times in the reactor. Then, heat the reactor for 72 h. After quenching, PPFPA homopolymer was obtained by methanol precipitation.

PPFPA homopolymer, NIPAM, and AIBN were dissolved in DMF and freeze-thaw four times in the reactor. Then, heat the reactor for 48 h. After quenching, PNIPAM-*b*-PPFPA block copolymer was obtained by methanol precipitation.

For the peptide substitution, Fmoc-Lys-OH and the diblock copolymer were dissolved in DMF, then adding TEA for 12 h in 60 ℃. After washing with water, the peptide substituted block copolymer was obtained.

Supporting Information

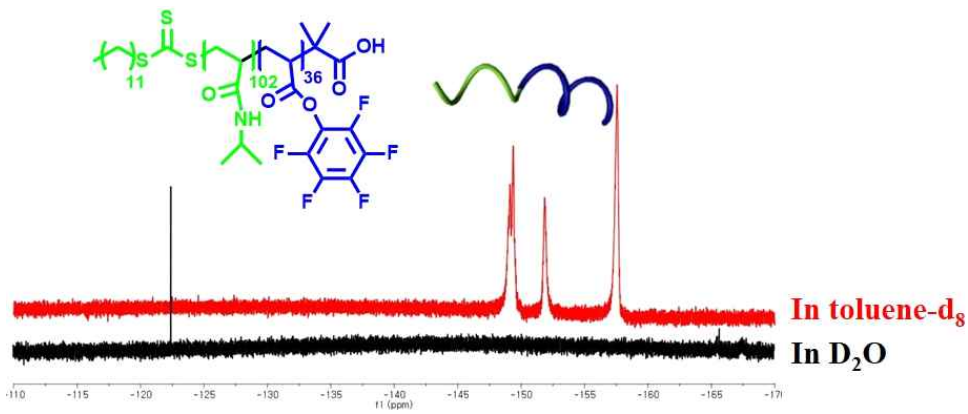

Figure S1. ^{19}F NMR of the diblock copolymer in D_2O and in toluene-d_8. In toluene, PPFPA block was exposed as a corona, so there were signal of fluorine in ^{19}F NMR.

References

(1) M. Jiang, *Polymer Chem.* 2014, *5*, 234-240.

Chapter 4. Preparing Water-Soluble Nanostructures of Polynaphthylene Vinylene Block Copolymers and Their Chemosensor Studies

Abstract

We demonstrate the nanostructures and chemosensor ability of the water-soluble block copolymers containing poly(naphthylene vinylene) (PNV) core block with some polyethylene glycol (PEG)-attached soluble corona blocks. The block copolymers of polyoxanorbornene-PEG with PNV formed the self-assembled nanostructures from nanospheres to nanorods by decreasing the soluble blocks in aqueous solution. Furthermore, poly (endo-tricyclo[4.2.2.0]deca-3,9-diene (TD)) with PEG soluble block and PNV BCPs formed the nanorods or unique fractal morphology with increasing the length of PEG. Furthermore, these water-soluble BCPs could be used in the chemosensor by using quenching fluorescence effect of the PNV block with 2,4,6-trinitrotoluene (TNT) in water. The efficiency of the chemosensor of the block copolymer (Stern-Volmer quenching constants (K_{sv})) was about 10^5 M^{-1}.

Introduction

Conjugated polymers have attracted interests to the researchers for many decades because of their semiconducting and good optoelectronic properties to use in many devices, such as chemosensors, solar cells, and field effect transistors. Among these conjugated polymers, the polymers of phenylene vinylene (PV) or naphthylene vinylene (NV) showed good electroluminescence properties, and used in many chemosensor fields, and were often called amplifying fluorescent polymers (AFPs)[1]. In AFPs, the solution-phase chemosensing ability have relied on the dimension or the nanostructures of block copolymers (BCPs) because there was a report showing a large morphological dependent sensor efficiency difference between the zero-dimensional 0D (nanosphere) and one-dimensional (1D) water-soluble nanostructures to the explosive 2,4,6- trinitrotoluene (TNT) sensing in aqueous solution[2]. As an extension of this result, we synthesized the water-soluble block copolymers incorporating new conjugated PNV core block with some polyethylene glycol (PEG) attached corona blocks and checked their chemosensor efficiency. Compared with PPV and PNV, PNV had a higher quantum yield than PPV because of the rigid conformation of polymer backbone[3]. Thus, we expected that the water-soluble BCPs composed of PNV might have a higher chemosensor efficiency than the previous PPV example.

Results and Discussion

Table 1. Synthesis of P(ONB-*b*-NV) BCPs.

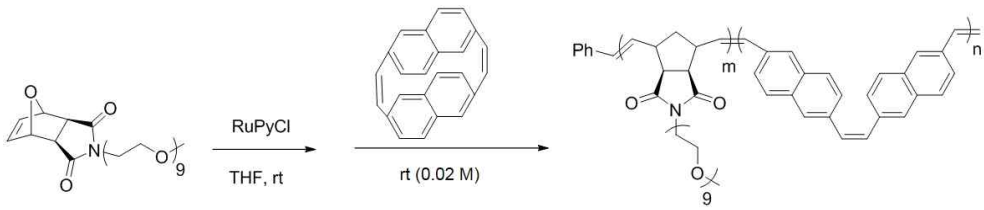

P(ONB-b-NV)	Time (ONB, NV)	Conv (%)	Yield (%)
30:20(PEG 9)	5 min, 12 h	100, 100	50
40:20(PEG 9)	5 min, 12 h	100, 100	55
50:20(PEG 9)	5 min, 12 h	100, 100	77
60:20(PEG 9)	5 min, 12 h	100, 100	86

At first, we selected an oxanorbornene block with adding PEG of DP 9 to solubilize the block copolymer with PNV in water. The block ratio of corona to core block was from 30:20 to 60:20. The block copolymers were synthesized by using third-generation Grubbs catalyst and showed the moderate yield and full conversion. The precipitation of the crude polymer was done in a cold ether at −78 ℃ condition using dry ice because of the sticky crude polymer.

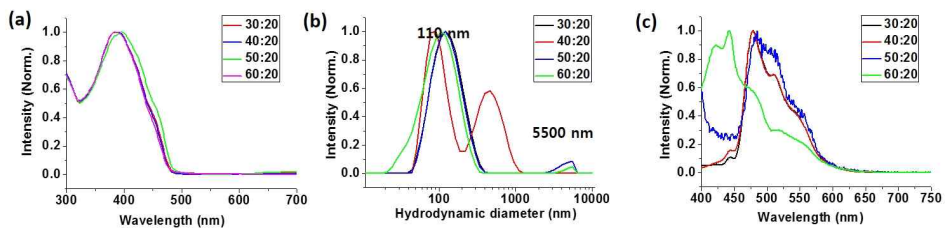

Figure 1. (a) UV-vis absorption spectra (0.05 mg/mL in water), (b) DLS data (1 mg/mL), and (c) fluorescence spectra (1 mg/mL) (excited by 400 nm) of P(ONB-*b*-NV) block copolymers with different DPs.

We first characterized the UV-vis absorption spectra, and the BCPs having same DP of NV block showed the similar absorption spectra with 400 nm λ_{max} which was typical λ_{max} for polynaphthylene vinylene or polyphenylene vinylene block (**Figure 1a**). The hydrodynamic diameters measured by dynamic light scattering (DLS) showed quite broad peaks from 110 nm to 5500 nm which might be coming from the irregular size of P(ONB-*b*-NV) nanostructures in aqueous solution (**Figure 1b**). However, the fluorescence spectra showed quite different peaks for the BCPs, and it seemed to be caused by the different nanostructures to have different emission peaks (**Figure 1c**).

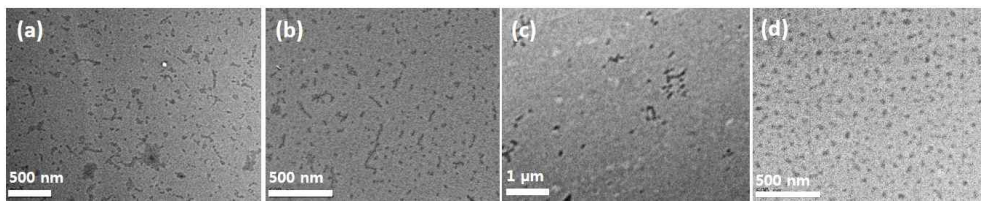

Figure 2. (a-d) TEM images of P(ONB-*b*-NV) BCPs with different DPs. (a) DP 30:20, (b) DP 40:20, (c) DP 50:20, and (d) DP 60:20 in aqueous solution 1 mg/mL.

The self-assembly structures of P(ONB-*b*-NV) BCPs from DP 30:20 to DP 60:20 were the aggregated nanorods, nanorods, shorter nanorods, and nanospheres each (**Figure 2**). Shorter soluble block induced less soluble and more aggregated nanostructures with exposure of insoluble core block, so DP 30:20 or DP 40:20 BCPs formed longer and more aggregated nanostructures than a longer soluble block (**Figure 2**).

Table 2. Synthesis of P(TD-*b*-NV) BCPs.

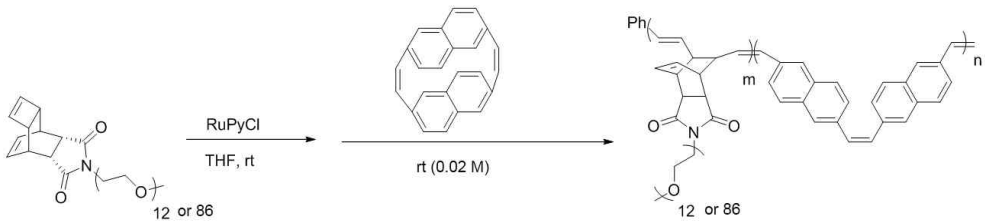

P(TD-*b*-NV)	Time (TD, NV)	Conv (%)	Yield (%)
20:20 (PEG 12)	5 min, 12 h	100, 100	52
20:40 (PEG 12)	5 min, 24 h	100, 100	66
5:40 (PEG 86)	5 min, 96 h	100, 100	62

We also changed the soluble block to endo-tricyclo[4.2.2.0] deca- 3,9-diene (TD) with modifying PEG length to DP 12 or DP 86. By using third-generation Grubbs catalyst at room temperature, we could achieve the BCPs with high conversions. However, the longer PEG chain caused more sticky of the crude polymer, so the yield was lower than P(ONB-*b*-NV). The block ratio of the corona (PEG DP 12) and core was 20:20 or 20:40 with increasing polymerization time of the second NV block for DP 40 about 24 h. In the case of TD-PEG DP 86 block, the polymerization time of the second block was increased much because of the long PEG blocks to suppress the addition of the second block to the propagating first block.

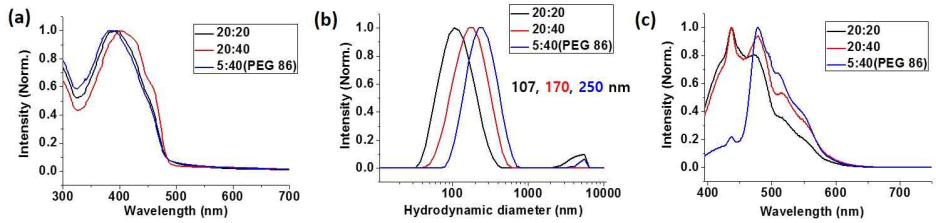

Figure 3. (a) UV-vis absorption spectra (0.05 mg/mL in water), (b) DLS data (1 mg/mL), and (c) fluorescence spectra (1 mg/mL) (excited by 400 nm) of P(TD-*b*-NV) BCPs with different DPs.

For the P(TD-*b*-NV) BCPs, they showed similar UV-vis absorption spectra with P(ONB-*b*-NV) BCPs with 400 nm λ_{max} (**Figure 3a**). In DLS, the BCPs also showed the broad hydrodynamic distributions with 100 – 250 nm distribution with a small portion of 5 μm size (**Figure 3b**). The fluorescence spectrum also showed similar trends for PEG 12 BCPs, and PEG 86 BCPs showed different peaks because of the different nanostructures (**Figure 3c**).

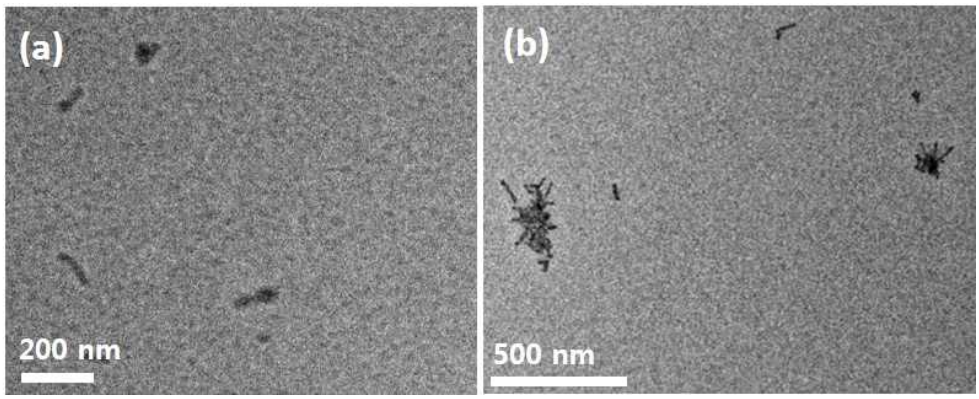

Figure 4. (a,b) TEM images of P(TD-*b*-NV) block copolymers with PEG DP of 12. (a) DP 20:20 and (b) DP 20:40 in aqueous solution (1 mg/mL).

The BCPs having TD-PEG 12 soluble block showed the nanorods (DP 20:20) or the aggregated nanorods (DP 20:40) by increasing insoluble second block (**Figure 4**).

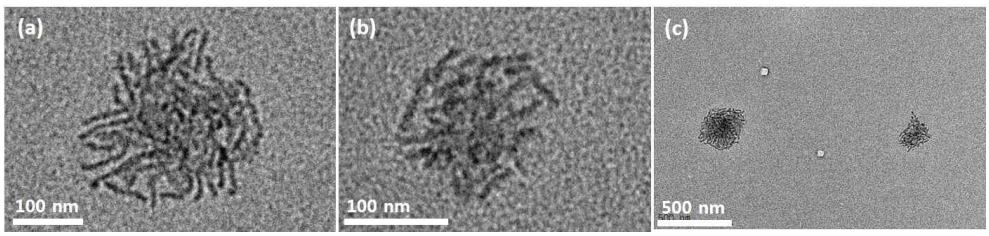

Figure 5. (a-c) TEM images of P(TD-*b*-NV) block copolymers with PEG DP of 86 in aqueous solution (1 mg/mL).

However, the BCPs containing longer PEG chain formed the branched nanostructures of the nanorods which were similar with the fractal morphology in water (**Figure 5**). This kind of unique fractal morphology might be originated from the uncontrolled polymerization of the naphthylene block which produced the micelles gradually attached each other *via* kinetic diffusion limited aggregation process[4,5]. The bulky TD-PEG 86 chain might induce the steric repulsion and the slow initiation of the second naphthylene block. Therefore, the uncontrolled and slow initiation of the insoluble PNV block to the propagating first block could induce the gradual generation of the micellar nanostructures instead of simultaneous self-assembly, and this phenomenon becomes the key point to the mechanism of the fractal formation.

Table 3. Stern-Volmer quenching constants (K_{sv}) of the water-soluble NV BCPs with PEGlated soluble blocks.

BCPs	DP	K_{sv} (M^{-1})
P(ONB-*b*-NV)	**30:20**	**3.33×10^5**
P(ONB-*b*-NV)	**40:20**	**2.86×10^5**
P(ONB-*b*-NV)	**50:20**	**1.60×10^5**
P(ONB-*b*-NV)	**60:20**	**1.47×10^5**
P(TD-*b*-NV) PEG DP 12	**20:20**	**8.03×10^4**
P(TD-*b*-NV) PEG DP 12	**20:40**	**1.08×10^5**
P(TD-*b*-NV) PEG DP 86	**5:40**	**1.71×10^5**

Then, we measured the quenching efficiency of the water-soluble BCPs containing electroluminescence NV block to an explosive 2,4,6-trinitrotoluene (TNT) in water (Table 3). In the case of P(ONB-*b*-NV), the Stern-Volmer quenching constants (K_{sv}) were about 1×10^5 to 3×10^5 M^{-1}, and these values were lower than the values of the previous PPV BCPs (3.9×10^5 M^{-1})[2]. There were still trends of longer 1D nanostructures showing better quenching efficiency than 0D nanostructures.

However, the morphology effect was not as dramatic as reported in the previous case which showed 20 times difference in K_{sv} value[2]. Furthermore, the K_{sv} of P(TD-*b*-NV) were about 1×10^5 M^{-1}, which were also lower than the previous report[2]. The fractal nanostructure had more surface area than nanorods or nanosphere. However, the increase of K_{sv} value was only 1.57 times difference compared with 1D nanorods. At now, it was hard to figure out the tendency of K_{sv} effect of these water-soluble PNV BCPs. Also, the higher quantum yield of PNV than PPV block did not affect much to

the chemosensor ability in the water-soluble BCPs and their nanostructures.

Conclusion

We demonstrated the water-soluble block copolymers containing PEG corona with electroluminescence polynaphthylene vinylene core blocks showing various nanostructures such as nanosphere, nanorod, and nanofractals with good quenching efficiency to the explosive in water. The Stern-Volmer quenching constants (K_{sv}) of the BCPs of PNV were about 10^5 M^{-1}, and these values were similar or less than the previous polyphenylene vinylene report. Therefore, the quenching efficiency was not simply determined by the different core block, but the other factors such as morphology of nanostructures, PEG length, or other factors might be more important to determine the K_{sv} values. Now, we are further studying about the relationship between the chemosensor efficiency and the nanostructure or chemical properties of water-soluble BCPs.

Experimental Section

Materials

Without additional notes, all reagents were commercially available from Sigma-Aldrich®, Tokyo Chemical Industry Co. Ltd., and Alfa Aesar®, and were used without further purification. THF for the polymerization was distilled over sodium and benzophenone, and degassed by Ar bubbling for 10 minutes before using.

General analytical information

NMR spectra were recorded by Varian/Oxford As-500 (500 MHz for ^{1}H and 125 MHz for ^{13}C) spectrometers. UV/Vis spectra were obtained by Jasco Inc. UV/vis Spectrometer V-550. Fluorescence spectra were obtained from FP-8300 (JASCO, USA). Dynamic light scattering (DLS) data were obtained by Malvern Zetasizer Nano ZS.

Transmission electron microscopy

TEM imaging was performed using JEM-2100 (JEOL) at 120 kV. The samples were prepared by drop casting one drop of the polymer solution (10 μL) on the Formvar and carbon-coated copper grid.

Experimental Procedure for Monomer Preparation

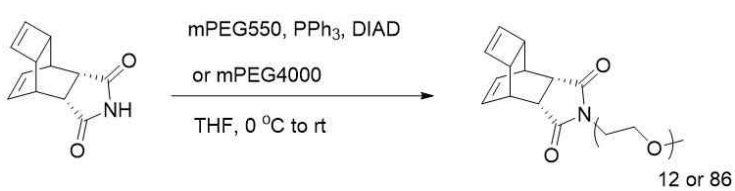

TD-NH^4 (2.48 mmol, 0.5 g) and PEG DP 12 (0.828 mmol, 0.5 g) was added to a dried flask, then catalytic amount of PPh_3 (3 mmol, 0.65 g) were added. The dried flasks were backfilled with Ar and evacuated three times, then degassed THF (50 mL) added *via* a syringe to dissolve them. After lowering the temperature to 0 ℃, diisopropyl azodicarboxylate (98%, 3 mmol, 0.49 mL) was added *via* a syringe. After stirring for 96 hours at room temperature, the mixture was quenched by the aqueous NH_4Cl solution. The crude product was evaporated without extraction process, and purified by flash column chromatography on silica gel (DCM: MeOH= 100:3) to afford compound TD-PEG 12 as an viscous liquid (0.441 g, 71 %). ^{1}H NMR (500 MHz $CDCl_3$): δ 5.91 (m, 4H), 3.67 (m, 48H), 3.40 (s, 3H), 3.18 (s, 2H), 2.80 (m, 4H).

The synthesis of TD-PEG 86 is same process with TD-PEG 12, but adding PEG DP 86 (average M_n: 4000 kDa) instead of PEG 12, and TD-PEG 86 was an white solid (2.78 g, 80 %). ^{1}H NMR (500 MHz $CDCl_3$): δ 5.95 (m, 4H), 3.57 (m, 350H), 3.40 (s, 3H), 3.27 (s, 2H), 2.80 (m, 4H).

Naphthylene vinylene was prepared through previously reported procedures[2].

ONB-PEG DP 9 was prepared through previously reported procedures[3].

TD-NH was prepared through previously reported procedures[4].

Preparation of diblock copolymers

A 5 mL sized screw-cap vial with a septum was flame dried and charged with the first monomer (soluble block) and a magnetic bar.

The vial was purged with argon four times, and degassed anhydrous THF was added. After the Ar-purged mixture of third-generation Grubbs catalyst in another flame dried 5 mL vial was dissolved in THF, the solution was rapidly injected to the solution of the first monomer at room temperature under vigorous stirring. After 5 min, the naphthylene vinylene was injected to the soluble block. The reaction was quenched by excess ethyl vinyl ether and partially precipitated in cold ether prepared by dry ice with acetone. Obtained viscous solid was dried *in vacuo*.

Poly(ONB-PEG_9)-*b*-poly(NV) block copolymers

^{1}H NMR (500 MHz, $CDCl_3$): δ 7.70 (br, 12H), 6.51 (br, 4H), 5.26 (br, 2H), 4.63 (br, 2H), 3.54 (br, 39H), 2.80 (br, 2H).

Poly(TD-PEG_{12})-*b*-poly(NV) block copolymers

^{1}H NMR (500 MHz, $CDCl_3$): δ 7.71 (br, 12H), 6.36 (br, 4H), 5.90 (br, 2H), 5.26 (br, 2H), 3.75 (br, 62H), 2.94 (br, 6H).

Poly(TD-PEG_{86})-*b*-poly(NV) block copolymers

^{1}H NMR (500 MHz, $CDCl_3$): δ 7.71 (br, 12H), 6.33 (br, 4H), 5.90 (br, 2H), 5.26 (br, 2H), 3.73 (br, 430H), 2.96 (br, 6H).

References

(1) Swager, T. M. *Chem. Rev.* 2007, *107*, 1339.
(2) Yu, C.-Y. J. *Polym. Sci. Part A: Polym. Chem.* 2018, *56*, 67.
(3) Choi, T.-L. *Polym. Chem.* 2017, *8*, 7507.
(4) Choi, T.-L. *J. Am. Chem. Soc.* 2018, *140*, 475.
(5) Sander, L. M. *Comtemp. Phys.* 2000, *41*, 203.

간단한 혼성화 동종 중합체의 결정화 주도 자기조립을 이용한 잘 정의된 나노구조의 제조

최 인 호
화학부 유기화학 전공
서울대학교 대학원

용액 상에서의 블록 공중합체의 자기조립현상은 수십 년간 이미 매우 많은 연구들로부터 잘 알려져 있으며, 이를 이용하여 다양한 나노구조들의 제조가 가능하였다. 이러한 나노구조들은 결정성이 좋은 코어 블록의 강한 상호작용 및 코로나 블록이 용매와의 상호작용으로 블록 공중합체 및 나노구조를 안정화시킬 수 있었기에 가능하였다. 그러나 간단한 펩타이드를 이용해 자기조립 구조를 만든 예시는 거의 없었다. 이에 본 논문에서는 간단한 펩타이드 혹은 펩타이드가 도입된 블록 공중합체를 이용하여 매우 균일하고 잘 정의된 나노구조를 만들었다.

또한 본 논문에서는 물에 잘 녹는 블록 공중합체를 고안하였으며, 이 블록 공중합체는 물에 잘 녹는 에틸렌글리콜 부분과 화학적 센서 기능을 가진 나프탈렌으로 이루어져 있다. 그리고 이 블록 공중합체가 좋은 형광 특성을 보임을 확인하였다.

핵심어: 펩타이드, 자기조립, 수용성 나노구조, 화학적 센서

학번: 2012-20290